Carbon and nitrogen isotope systematics in diamond: different sensitivities to isotopic fractionation or a decoupled origin?

K. Hogberg[1*], T. Stachel[1], R.A. Stern[1]

[1] Canadian Centre for Isotopic Microanalysis, Department of Earth and Atmospheric Sciences, University of Alberta, Edmonton, AB, Canada, T6G 2E3

* Corresponding author: hogberg@ualberta.ca

Keywords:

Diamond
Carbon isotopes
Nitrogen isotopes
Rayleigh fractionation
Chidliak
Hall Peninsula

Abstract

Using stable isotope data obtained on multiple aliquots of diamonds from worldwide sources, it has been argued that carbon and nitrogen in diamond are decoupled. Here we re-investigate the carbon-nitrogen relationship based on the most comprehensive microbeam data set to date of stable isotopes and nitrogen concentrations in diamonds (n=94) from a single locality. Our diamond samples, derived from two kimberlites in the Chidliak Field (NE Canada), show large variability in $\delta^{13}C$ (-28.4 ‰ to -1.1 ‰, mode at -5.8 ‰), $\delta^{15}N$ (-5.8 to +18.8 ‰, mode at -3.0 ‰) and nitrogen contents ([N]; 3800 to less than 1 at.ppm). In combination, cathodoluminescence imaging and microbeam analyses reveal that the diamonds grew from multiple fluid pulses, with at least one major hiatus documented in some samples that was associated with a resorption event and an abrupt change from low $\delta^{13}C$ and [N] to mantle-like $\delta^{13}C$ and high [N]. Overall, $\delta^{13}C$ appears to be uncorrelated to $\delta^{15}N$ and [N] on both the inter- and intra-diamond level. Co-variations of $\delta^{15}N$-log[N], however, result in at least two parallel, negatively correlated linear arrays, which are also present on the level of the individual diamonds falling on these two trends.

These arrays emerge from the two principal data clusters, are characterized by slightly negative and slightly positive $\delta^{15}N$ (about -3 and +2 ‰, respectively) and variable but overall high [N].

Using published values for the diamond-fluid nitrogen isotope fractionation factor and nitrogen partition coefficient, these trends are perfectly reproduced by a Rayleigh fractionation model. Overall, three key elements are identified in the formation of the diamond suite studied: (1.) a low $\delta^{13}C$ and low [N] component that possibly is directly associated with an eclogitic diamond substrate or introduced during an early stage fluid event. (2.) Repeated influx of a variably nitrogen-rich mantle fluid (mildly negative $\delta^{13}C$ and $\delta^{15}N$). (3.) In waning stages of influx, availability of the mantle-type fluid at the site of diamond growth became limited, leading to Rayleigh fractionation. These fractionation trends are clearly depicted by $\delta^{15}N$-[N] but are not detected when examining co-variation diagrams involving $\delta^{13}C$. Also on the level of individual diamonds, large (≥5 ‰) variations in $\delta^{15}N$ are associated with $\delta^{13}C$ values that typically are constant within analytical uncertainty. The much smaller isotope fractionation factor for carbon (considering carbonate- or methane-rich fluids as possible carbon sources) compared to nitrogen leads to an approximately one order of magnitude lower sensitivity of $\delta^{13}C$ values to Rayleigh fractionation processes (i.e. during fractionation, a 1 ‰ change in $\delta^{13}C$ is associated with a 10 ‰ change in $\delta^{15}N$). As a consequence, even minor heterogeneity in the primary isotopic composition of diamond forming carbon (e.g., due to addition of minor subducted carbon) will completely blur any possible co-variations with $\delta^{15}N$ or [N]. We suggest this strong difference in isotope effects for C and N to be the likely cause of observations of an apparently decoupled behaviour of carbon and nitrogen isotopes in diamond.

1. Introduction

The recycling of crustal carbon and nitrogen into the deep mantle and the role of mantle-derived versus subducted carbon and nitrogen in diamond genesis have long been a subject of intense scientific debate (Sobolev and Sobolev, 1980; Javoy et al., 1986, Cartigny et al., 1998; Deines, 2002, Mikhail et al., 2014). In particular, the absence of a correlation between ^{13}C depletion (the signature of original organic matter) and ^{15}N enrichment (characteristic for sediments) in diamonds has been used as an argument against an involvement of subducted carbon and

nitrogen (see review in Cartigny, 2005). This argument, however, critically hinges on a common origin of carbon and nitrogen in diamond; this supposition was recently challenged by Mikhail et al. (2014), principally based on the much larger heterogeneity of $\delta^{15}N$ compared to $\delta^{13}C$ in their sample suite. A recent empirical determination of a nitrogen isotope fractionation factor for diamond-fluid (Petts et al., 2015) now allows us to re-examine the relationship of carbon and nitrogen in diamond. For this purpose, we undertook the first microbeam $\delta^{13}C$–$\delta^{15}N$–[N] study based on a representative number (n=94) of diamond samples from a single occurrence; this comprehensive data set allows us to re-evaluate the two conflicting proposals regarding coupled (Cartingy et al., 1998) or decoupled (Mikhail et al., 2014) carbon and nitrogen isotope systematics in diamond.

Carbon isotopic analysis is a standard tool for monocrystalline diamond studies and may be employed to fingerprint the original diamond substrate in Earth's mantle (peridotitic versus eclogitic or websteritic paragenesis; Kirkley et al., 1991; Stachel et al., 2009). The frequency distributions of diamonds of peridotitic and eclogitic (-websteritic) paragenesis both share a common mode in $\delta^{13}C_{VPDB}$ at -5 ±1 ‰ ("mantle value" of carbon; Deines, 1980; Cartigny, 2005). Diamonds of peridotitic paragenesis, however, have a much narrower range in carbon isotopic composition (with rare exceptions, they generally fall between about -10 and 0 ‰) than eclogitic diamonds (-41 to +5 ‰) (e.g., Kirkley et al., 1991; Cartigny, 2005; Stachel et al., 2009), and consequently $\delta^{13}C$ values that extend past the range of peridotitic diamonds can be attributed with fairly high confidence to eclogitic (-websteritic) substrates.

As carbon and nitrogen have a similar ionic radius and charge, nitrogen substitutes for and bonds strongly with carbon in the diamond lattice (Cartigny, 2005); as a consequence, nitrogen is by far the most abundant molecular impurity in diamond, with concentrations as high as 0.55 wt. % (Sellschop et al., 1980). This enables utilising the content and isotopic composition of nitrogen as an additional tool to obtain broad constraints on the mantle substrate(s) of a suite of diamonds. For example, globally, peridotitic diamonds are typically much lower in nitrogen content (median of 82 at.ppm) than eclogitic diamonds (median of 494 at.ppm; Stachel, 2014). The nitrogen content of the mantle is much lower than the carbon content; estimates for primitive upper mantle N fall between 2 ppm (Marty, 1995) and 36 ppm (Javoy, 1997), with the latter value likely representing an extreme upper limit (Cartigny and Marty, 2013). Depleted mantle (MORB source) contains about 0.3 ppm nitrogen (Marty and Dauphas, 2003; Johnson and

Goldblatt, 2015). Due to the low quantities of nitrogen in the upper mantle, coupled with a large extent of nitrogen recycling in the course of subduction (Cartigny and Marty, 2013), $\delta^{15}N$ is a sensitive recorder of mixing between isotopically highly distinctive mantle and crustal reservoirs. The mantle value for $\delta^{15}N$ is -5 ±3 ‰ (Nadeau et al., 1990; Cartigny, 2005), whereas crustal reservoirs are characterized by positive $\delta^{15}N$ values (e.g., Peters et al., 1978; Cartigny and Marty, 2013). Therefore, a subducted crustal nitrogen component is traceable in mantle plume-related magmas and some mantle xenoliths (Marty and Dauphas, 2003) and may reflect the presence of an important additional, high-nitrogen mantle reservoir with a nitrogen isotopic composition of about +5 ‰ (Johnson and Goldblatt, 2015).

Here we present the first study on diamonds from the recently discovered Chidliak kimberlite field (Pell et al., 2012 and 2013) in NE Canada. The Chidliak kimberlites are located on the Hall Peninsula, southern Baffin Island, an area that was originally considered part of the Churchill Province but is now recognized as an independent Archean cratonic block, possibly representing a fragment of the North Atlantic Craton (Pell et al., 2013 and references therein). To date, 74 kimberlites have been discovered and of the 51 kimberlites tested, 21 contain "commercial-sized" (>850 µm) diamonds (J. Pell, pers. comm., 2015). In this study we focus on diamonds from two kimberlite bodies, CH-7 (kimberlite sample P5500) and CH-6 (kimberlite sample P6807).

2. Sample description and experimental methods

We inspected 210 Chidliak diamonds for their physical characteristics; the upper stone size is -850 µm +650 µm (aperture size of upper and lower sieves) and the lower stone size is -300 µm +212 µm. Half of the diamonds are from kimberlite CH-7, the other half from CH-6. The studied diamonds are predominantly irregular (a common feature of very small diamonds), followed by octahedral fragments. Dodecahedroids, cuboids, macles, aggregates and mixed octahedral-dodecahedral morphologies are also present. The majority of the diamonds is colorless, followed by brown, yellow, and grey.

A subset of 94 diamonds, in the size range of 850 µm to 300 µm, was analysed via secondary ion mass spectrometry (SIMS) with high spatial resolution (15 µm spot size). All analytical data are summarized in Table 1. $\delta^{13}C$ (the $^{13}C/^{12}C$ ratio expressed as relative difference

to the same value in the Vienna PeeDee Belemnite standard) and nitrogen contents ([N]) were analysed for all 94 diamonds, whereas $\delta^{15}N$ values (the $^{15}N/^{14}N$ ratio expressed as relative difference to the same value for standard atmosphere) could only be obtained for 85 diamonds having nitrogen contents >40 at.ppm. Prior to SIMS analysis, the diamonds were mounted in epoxy, polished and then imaged by cathodoluminescence (CL). Due to mounting procedures, the imaged diamonds could not be oriented in specific crystallographic directions. In addition, as multiple diamonds were polished in single mounts, sections through crystal centres were only achieved in rare cases. The consequent random sections through mainly outer parts of diamond crystals introduce complexity to the CL images.

MC-SIMS (Cameca IMS-1280) analyses of diamond follow the procedures outlined in Stern et al. (2014); the reference materials used for $\delta^{13}C$ analysis were diamonds S0011Bd and S0011Cd, while the reference diamond used for $\delta^{15}N$ analyses was S0270. After $\delta^{13}C$ analysis, the nitrogen content was measured on the same spot location (N_C in Table 1); $\delta^{15}N$ was measured on adjacent spots but within the same diamond growth layer and a second nitrogen content value (N_N in Table 1) was obtained during these analyses. The error on the nitrogen content measurements is ±10 %, which is largely due to the uncertainty of the FTIR analysis of the reference material.

Following SIMS analysis, all analytical spots were verified using a light microscope and the CL and SE (secondary electron) images to ensure (1.) the absence of surface contamination (one analyses was removed due to possible epoxy contamination) and (2.) that analytical spots are located within single growth layers (three analyses were removed as they overlapped boundaries between distinct growth zones). Since nitrogen content was always measured on two adjacent spots, associated with the $\delta^{13}C$ and $\delta^{15}N$ analyses, all paired nitrogen values that did not agree within error prompted re-examination of correct placement of the adjacent spots within the same growth layer; this led to the recognition of two pairs of spots where $\delta^{13}C$ and $\delta^{15}N$ were obtained on different sides of important growth boundaries (associated with changes in $\delta^{13}C$ >3 ‰). The $\delta^{13}C$ and $\delta^{15}N$ values associated with these two pairs of spots are listed in Table 1 (highlighted by a *) as they are accurate analyses within individual layers but they are not used to examine co-variations in $\delta^{13}C$-$\delta^{15}N$.

3.0 Results

3.1 Carbon isotopic composition

Multiple points (2-7, average of 3 points) per diamond were measured. Diamonds from the two kimberlites have subtly distinct principle modes (defined using probability density curves; Ludwig, 1999): -5.8 ‰ for CH-7 and -6.4 ‰ for CH-6. Combined, these diamonds show a range in $\delta^{13}C$ between -28.4 and -1.1 ‰, with a principle mode at -5.8 ‰, near the value of mantle carbon (-5 ±1 ‰; Deines, 1980; Cartigny, 2005), and minor modes about -15.5 ‰ and -23.5 ‰ (Fig. 1A; Table 1).

3.2 Nitrogen content and isotopic composition

Nitrogen contents (N_C, i.e. measured on the same analytical spots as $\delta^{13}C$) for the diamonds studied range from <1 to 3833 at.ppm with a median value of 1112 at.ppm (Fig. 2). Compared to diamonds worldwide, median [N] values are high for diamonds from the two kimberlites: 1092 at.ppm for CH-7 and 1260 at.ppm for CH-6 diamonds; a distinct low-N population is, however, present as well.

The nitrogen isotopic compositions ($\delta^{15}N$) of diamonds from the two kimberlites have similar ranges (-5.6 to +18.8 ‰ for CH-7 and -5.8 to +15.7 ‰ for CH-6) but distinct modes (-2.8 ‰ for CH-7 and +3.3 ‰ for CH-6). Combined, $\delta^{15}N$ of diamonds from both kimberlites ranges from -5.8 to +18.8 ‰ with a principle mode about -3.0 ‰ and secondary modes at +3.1 ‰ and +6.5 ‰ (Fig. 3A).

4. Discussion

4.1 Relationships between CL patterns, $\delta^{13}C$, N content and $\delta^{15}N$

Luminosity differences in the CL images of diamonds relate to differences in concentrations of impurities (e.g., nitrogen in N3 centres) and defects (e.g., Wilks and Wilks, 1991). Therefore, CL imaging makes the identification of internal growth structures possible wherever such impurities or defects are present. Identified types of growth patterns for CH-6 and CH-7 diamonds include:

(1.) "*hiatus*", (2.) "*homogenous*", (3.) "*agate-like banding*", (4.) "*octahedral*", (5) "*cuboid*" and (6.) "*complex*" (Fig. 4). *Hiatus*-type patterns involve abrupt, strong changes in CL response across sharp resorbed boundaries, and in this study are typically accompanied by distinct outward (across the boundary) changes from very negative to mantle-like $\delta^{13}C$ values and a significant increase in nitrogen content. Diamonds with *homogenous* CL lack prominent internal features and typically lack significant variation in $\delta^{13}C$, nitrogen content or $\delta^{15}N$. *Agate-like banding* comprises multiple narrow growth bands that may coincide with small variations in $\delta^{13}C$, $\delta^{15}N$ and nitrogen content. *Octahedral* and *cuboid*-type CL patterns reveal the symmetry of the internal growth, based on a combination of angles between growth sectors and a hummocky appearance of cuboid growth (diamond CH6-3 in Fig. 4). *Complex*-type CL patterns are characterised by irregular or "chaotic" internal growth structures.

The hiatus-style CL patterns (n=4 stones) document two separate diamond forming episodes with distinct $\delta^{13}C$ and [N] signatures: (1.) earlier grown diamond with $\delta^{13}C$ between -24.2 and -22.1 ‰, N contents from 0.4 to 119 at.ppm, and $\delta^{15}N$ between -1.5 to +6.9 ‰ (only determined for two diamonds with sufficiently high N contents for $\delta^{15}N$ analyses). (2.) Overgrowth of diamond with $\delta^{13}C$ from -6.4 to -3.4 ‰, N contents of 647 to 1616 at.ppm, and $\delta^{15}N$ between -5.0 to -1.0 ‰. The initial diamond growth could have acted as a seed diamond for the later diamond overgrowths, after a period of resorption. Distinct diamond-forming episodes have also been identified using CL in the studies of Palot et al. (2013, 2014).

Small-scale fluctuations in $\delta^{13}C$ of up to 3 ‰ (12 diamonds without evidence of resorption between growth layers have internal variations >1 ‰) across regular growth zones visible in CL images suggest either involvement of multiple fluid/melt pulses or diamond precipitation from an evolving medium.

4.2 Co-variations between carbon isotopes and nitrogen abundances

$\delta^{13}C$ frequency distributions skewed to ^{13}C depleted values (<-10 ‰) are characteristic for eclogitic diamond populations (e.g., Deines, 1980; Kirkley et al., 1991; Cartigny et al, 2001; Stachel and Harris, 2009). This characteristic skewness is also observed for the Chidliak diamond suite, documented by a prominent tail to ^{13}C-depleted compositions, and shows overall

good agreement with the carbon isotopic distributions of eclogitic diamonds from both Canadian and worldwide sources (Fig. 1).

Nitrogen contents in the diamonds from the CH-6 and CH-7 kimberlites (Fig. 2) show a bimodal distribution, with frequency maxima in classes 0-200 at. ppm and 1000-1200 at.ppm, the latter coinciding with the median value of 1112 at.ppm. For deposits worldwide, such high nitrogen contents are typically but not invariably associated with diamonds of the eclogitic suite (see section 1 and Fig. 2). Combined with the independent observation of strongly ^{13}C depleted diamonds at Chidliak, however, the overall high nitrogen contents suggest the presence of a large to dominant eclogitic component. Indicator mineral work on the Chidliak kimberlites (Neilson et al., 2012; Pell et al. 2013) exclusively links diamonds to counts of eclogitic (-websteritic) garnets (classes G3D and G4D of Grütter et al., 2004) and specifically not to the abundance of harzburgitic garnets (class G10D), independently firmly corroborating an eclogite-based mineralization model for Chidliak.

For diamonds worldwide, a relationship of decreasing maximum nitrogen content with decreasing $\delta^{13}C$ has been well established (Stachel and Harris, 1997) and was termed "limit sector" by Cartigny et al. (2001). The Chidliak diamond suite roughly follows this general trend (Fig. 5), but within individual diamonds (e.g., samples CH6-2 and CH7-39), decreasing $\delta^{13}C$ is in some instances associated with increasing nitrogen content. Similar observations of diamond internal trends oblique to the "limit sector" have previously been made elsewhere (e.g., Smart et al., 2011; Palot et al., 2013, Wiggers de Vries et al., 2013).

The analytical points constituting the prominent mode in $\delta^{13}C$ between -8 to -2 ‰ (Fig. 1) appear to form a continuous trend from high to low nitrogen concentrations in Figure 5 but overall establish the bimodal distribution in nitrogen content shown in Figure 2.

4.2.1 The origin of ^{13}C-depleted diamond carbon

A relatively small number of analyses (17%) yielded $\delta^{13}C$ values below -10 ‰, with half of these falling below -20 ‰. The origin of strongly ^{13}C depleted diamonds has long been linked to subducted organic matter, probably associated with intensely sea water altered uppermost MORB (Sobolev and Sobolev, 1980; Kirkley et al, 1991; McCandless and Gurney, 1997; Tappert et al., 2005). Alternative explanations link strong ^{13}C depletion to fractionation

processes at high temperature within Earth mantle (Cartingy et al., 2001; Mikhail et al., 2014). Studies on the oxygen isotope composition of mineral inclusions in diamonds with strongly negative $\delta^{13}C$ from four locations worldwide have, however, invariably shown an association with significant ^{18}O enrichment (Schulze et al., 2003 and 2013; Ickert et al., 2013 and 2015), lending strong support to the subduction hypothesis. As a consequence, we consider our diamond analyses yielding $\delta^{13}C$ values below -20 ‰ to reflect predominantly subducted former organic matter, whilst values between -10 to -20 ‰ may represent mixing of subducted and mantle-derived carbon.

For the bulk of the studied diamonds, however, $\delta^{13}C$ is greater than -10 ‰ and 78% of all analyses fall between -8 to -2 ‰, the "mantle range" of Cartigny (2005). Although we infer a predominantly eclogitic association of the Chidliak diamond suite (see above), we certainly would not exclude that the majority reflect mantle-derived carbon (c.f. Taylor et al., 1998; Ickert et al. 2013; Cartigny et al., 2014)

4.3 $\delta^{13}C$–$\delta^{15}N$ and $\delta^{15}N$–[N] relationships

No systematic co-variations between $\delta^{13}C$ and $\delta^{15}N$ are observed on the scale of either individual diamonds or the entire diamond population studied (Fig. 6, Table 1). The overall spread in $\delta^{15}N$ values decreases with increasing ^{13}C depletion, likely reflecting a strong decrease in sample density in the same direction.

For $\delta^{15}N$–log[N] (Fig 7A), the most prominent feature is the large variability in nitrogen content among diamonds with isotopic compositions that correspond to the main mode in Figure 3 ($\delta^{15}N$ between about -5 to 0 ‰). Based on the premise that the concentration of nitrogen in diamond relates to the concentration of nitrogen in the diamond forming fluid (see section 4.3.3), variable degrees of dilution of isotopically fairly homogenous nitrogen (e.g., through a silicate or carbonate melt component, or H_2O) could establish such a process. A subset of diamonds extending to positive $\delta^{15}N$ values forms sub-parallel trends of decreasing nitrogen content with increasing $\delta^{15}N$ (Fig. 7A) that are also visible on the scale of individual diamonds (Fig. 7B). On the intra-diamond level, the trends depicted in Figure 7B are not present in the form of systematic core-rim variations; this likely relates to the fact that only a few spots (average of 3) per diamond were analyzed, which probe distinct growth events (c.f., Wiggers de Vries et al.,

2013; Bulanova et al., 2014) rather than systematic outward zonations that typically are restricted to within individual growth zones. The presence of non-chronological $\delta^{15}N$–[N] trends on the level of individual diamonds is interpreted to reflect operation of the same evolutionary process through repeated events. In any case, the presence of the sub-parallel intra-diamond trends clearly validates their existence on the level of multiple diamonds.

Possible explanations for the observed negative correlations between nitrogen content and $\delta^{15}N$ include: (1.) Mixing of nitrogen derived from two components with distinct nitrogen concentrations and isotopic compositions. (2.) Isotopic fractionation and nitrogen loss prior to diamond crystallization. (3.) Rayleigh fractionation during diamond precipitation.

4.3.1 Mixing between reservoirs

Mixing between two components, one with a mantle-like nitrogen isotopic composition and strongly variable but mostly high nitrogen content, and a second with highly positive $\delta^{15}N$ and low nitrogen content could generate the subparallel trends seen in Figure 7. The large variability of carbon isotopic compositions in this sample set may require inclusion of additional components (Fig. 6), e.g., a contribution of oceanic crust-derived organic matter. For the sake of simplicity here we focus our discussion exclusively on samples with "mantle-like" $\delta^{13}C$ (between -10 ‰ and the maximum sample value of -1.1 ‰, constituting 83% of the available data points). For these samples, two extended linear arrays are apparent in Figure 8, originating from the two main clusters of diamond compositions, one at very high [N] (~3000 at.ppm) and slightly positive $\delta^{15}N$ (~2 ‰), the other at more variable but on average lower [N] (~1500 at ppm) and slightly negative $\delta^{15}N$ (~-3 ‰). Figure 7B shows that diamonds falling on the two linear arrays have internal $\delta^{15}N$–log[N] co-variations that mimic the overall trends.

Isolating one of the two linear arrays displayed by samples with mantle-like $\delta^{13}C$ (Fig. 8) allows to specifically test for an origin via either two component mixing or Rayleigh fractionation. In a non-logarithmic diagram, mixing of two components with different N content and $\delta^{15}N$ results in mixing hyperbolae that resemble the curved nature of a Rayleigh fractionation trends (Faure, 1986; Mariotti et al., 1988). Plotting the reciprocal nitrogen concentration versus $\delta^{15}N$ (Fig. 9) will, however, transform a mixing hyperbola into a straight line whilst the exponential nature of Rayleigh fractionation still produces a curved relationship

(Faure, 1986). The exponential trend shown in Figure 9, therefore, clearly precludes mixing as the cause of the $\delta^{15}N$–log[N] co-variations seen among the studied diamonds.

4.3.2 Open system isotope fractionation preceding diamond growth

During warm subduction, NH_4^+ residing in K-bearing minerals may be released into fluids as N_2 or NH_3, associated with progressive ^{15}N enrichment in the residual rock (Haendel et al. 1986; Bebout and Fogel 1992; Busigny and Bebout, 2013). The expected increases in $\delta^{15}N$ are, however, almost an order of magnitude smaller than observed in our sample set (Busigny and Bebout, 2013).

Cartigny et al. (2001) proposed that N may be lost together with CO_2 during separation of a fluid phase from a carbonate-bearing melt prior to diamond precipitation. To explain the co-variations of [N] and $\delta^{15}N$ seen in Figure 8, N loss from the diamond precipitating fluid would need to be accompanied by isotope fractionation. Indeed, isotopic analysis of vesicles and associated fresh MORB glasses suggests that degassing at magmatic temperatures is associated with $\Delta^{15}N_{vesicle\text{-}melt}$ of -1.6 ‰ (Cartigny et al., 2001b). A subsequent study (Fischer et al., 2005) on arc lavas and ocean island basalts, however, showed no systematic nitrogen isotope fractionation between linked olivine separates and gas samples, implying that magma degassing is not associated with N isotope fractionation. Yokochi et al. (2009) showed the potential for large kinetic isotope effects during diffusive nitrogen exchange between xenolith phlogopite and the host magma. Strong kinetic isotope effects at temperatures of the deep diamond-stable lithospheric mantle are, however, not considered likely. Nitrogen isotope fractionation during fluid separation under mantle conditions (high P and T) is currently unresolved, but if existent, any possible fractionation effects are expected to be small (Marty and Dauphas, 2003). Such a scenario is, therefore, not further considered here.

As an alternative, potential isotope effects associated with changes in the speciation of nitrogen at mantle conditions need to be evaluated. The speciation of nitrogen changes with temperature, pressure and oxygen fugacity. In oceanic sediments, nitrogen is released as NH_3 into pore fluids during biological and thermal degradation of organic matter, converted to NH_4^+ and incorporated into clay minerals, while the isotope signature of organic matter is largely retained (Thomazo and Papineau, 2013). During subduction and associated metamorphism of

sediments, NH^{4+} may be transferred from clay minerals into the crystal lattices of newly formed K-bearing minerals that are stable to great depth, such as micas (e.g., phengite; Busigny et al., 2003), hollandite (Watenphul et al., 2009) and clinopyroxene (Watenphul et al., 2010). Alternatively, prograde devolatilization may occur, releasing nitrogen as NH_4^+, which under oxidizing conditions in subducted sediments will be converted to N_2 (Duit et al., 1986). Under the conditions of diamond formation (high pressure, "cool" cratonic geotherm and reducing conditions) nitrogen in a fluid phase was experimentally shown to be principally NH_3 (Li and Keppler, 2014). In a computational study incorporating pH, Mikhail and Sverjensky (2014), however, found that under typical diamond stable conditions nitrogen in aqueous fluids would predominantly be present in the form of NH_4^+. Possible speciation changes from ammonium to ammonia would be associated with significant isotopic effects, with $\Delta^{15}N_{NH4+ - NH3}$ in the order of 3.0 to 1.7 (calculated at 900 and 1300 °C, respectively), whilst speciation changes involving N_2 would have more modest impact, with $\Delta^{15}N_{NH4+ - N2}$; of 1.9 to 1.1 and $\Delta^{15}N_{NH3 - N2}$ of -1.1 to -0.6 (again at 900 and 1300 °C, respectively; calculations based on Table 2 of Petts et al., 2015, with input data from Richet et al. 1977; Martin et al. 1992; Martin and Lee, 1996). Of these possible reactions, only two could drive the residual fluid in the direction observed in Figure 8, i.e. increasing $\delta^{15}N$ and decreasing N content: (1.) Protonation of ammonia to ammonium and (2.) oxidation of NH_3 to N_2. Protonation of NH_3 could occur during mixing of a dry nitrogen-bearing fluid and an acidic hydrous fluid. To achieve both large isotopic effects and a simultaneous decrease in nitrogen content (Fig. 8), such a process would need to occur in an open system with continuous loss of NH_4^+. To predict loss of the ionized species ammonium rather than ammonia from the mixed fluid is counterintuitive. The alternative, open system oxidation of NH_3 to N_2, which continuously has to escape from the diamond forming fluid, also is geologically unlikely. Firstly, it is unclear how such a dry fluid (in a hydrous fluid NH_4^+ rather than NH_3 would be expected; Mikhail and Sverjensky, 2014) could achieve the metasomatic effects (re-enrichment in mantle incompatible elements) that appear to be invariably associated with diamond formation (Stachel and Harris, 1997; Stachel and Luth, 2015). Secondly, $\Delta^{15}N_{NH3 - N2}$ is too small to explain the observed isotope effect (~18 ‰ variation, Fig. 8) without requiring unreasonably high levels of fractionation.

4.3.3 Rayleigh fractionation during diamond precipitation

Rayleigh fractionation in fluid limited systems has previously been invoked to explain co-variations of nitrogen content and $\delta^{13}C$ in diamond sample populations (e.g., Cartigny et al., 2001; Thomassot et al., 2007; Stachel and Harris, 2009) and across individual diamond growth zones (e.g., Bulanova et al., 2002; Zedgenizov et al., 2006; Smart et al., 2011). The distribution of nitrogen between diamond and its growth medium is still a matter of debate (e.g., Boyd et al. 1994; Cartigny et al., 2014; Mikhail and Howell, 2016). Empirical evidence, however, indicates, that wherever smooth compositional trends are observed (e.g., during in situ analysis of individual diamond plates), they are associated with nitrogen depletion during diamond growth and, by inference, a compatible behavior (e.g., Thomassot et al., 2007; Reutsky et al., 2008; Stachel et al., 2009; Smart et al., Wiggert de Vries 2013, Palot et al., 2014). Obtained values for the partition coefficient of nitrogen (K_N) between diamond and fluid vary between 2–5 for lithospheric (Thomassot et al., 2007; Stachel et al., 2009; Smart et al., 2011; Wiggert de Vries 2013) and 4–16 for sublithospheric diamonds (Palot et al. 2014), with only a minor or no dependence on oxygen fugacity (ranging from methane- to carbonate-bearing systems for natural diamonds and highly reducing conditions for high pressure–high temperature synthesis). For the studies suggestive of a possible relationship between K_N and fO_2 (e.g., Stachel et al., 2009), the compatibility of nitrogen in diamond decreases only moderately from carbonate- to methane-rich fluids. Partition coefficients of nitrogen between diamond and fluid are typically derived from the regression of linear covariations of $\delta^{13}C$ and log[N] and, by equating the amount of residual fluid left to the amount of residual carbon species left, implicitly assume diamond precipitation from a pure methane or carbonate fluid (see Petts et al., 2015, p. 192 for a detailed discussion). Here we adopt a K_N value of 4.4 constrained for diamond precipitation from a pure carbonatitic fluid (Petts et al., 2015). Nitrogen-based mantle residence temperatures (calculated after Leahy and Taylor, 1997, assuming 1 Ga mantle residence) for 80% of the studied Chidliak diamonds fall between 1050-1150°C (average of all samples is 1090°C; Nichols, 2014), bracketing the temperature, 1100°C, used to derive the nitrogen isotope fractionation factor of Petts et al. (2015). Diamond forming fluids likely are not pure carbon species (carbonate, CO_2 or CH_4) but may contain, e.g., H_2O or dissolved solids, which would act to increase the determined nitrogen partition coefficient of Petts et al. (2015) and also in the other studies cited above. If the dilution of the carbon species in the diamond forming fluid beneath Chidliak was, however, of similar

magnitude as for the natural (Jericho) diamond used by Petts et al. (2015), this potential underestimate of K_N would become irrelevant with respect to the slope of $\delta^{13}C$–log[N] co-variations (the degree of fractionation would, however, represent an upper estimate). An additional complicating aspect is that the partitioning of both carbon and nitrogen is not necessarily controlled exclusively by diamond as the only precipitating solid, but other phases such as carbonates (for C) or K-bearing phases (for N) may co-precipitate or be consumed during diamond formation, i.e. the behavior of C and N would need to be described by bulk distribution coefficients rather than diamond-fluid partitioning only. However, the modal composition of the co-precipitating mineral assemblage cannot be constrained from diamond analyses only.

For carbon isotope fractionation, reduced and oxidized fluid species have to be considered, with the isotope fractionation factor $\Delta^{13}C_{\text{diamond - fluid}}$ varying from -3.7 ‰ (CO_2), over -1.7 ‰ (CO_3^{2-}) to +1.1 ‰ (CH_4) (at T=1100 °C after Bottinga, 1969; Richet et al., 1977; Deines, 1980; Chacko et al., 1991; Smart et al., 2011). Among the oxidized carbon species, only carbonate is usually considered for diamond formation, due to both a strong link between carbonatitic high density fluids and diamond growth established through fluid inclusion studies (Navon et al., 1988; Weiss et al., 2014) and the buffering (i.e. immobilization as carbonate) of CO_2 by mantle olivine (Wyllie and Huang, 1976).

The derivation of an isotope fractionation factor for nitrogen (at 1100 °C, $\Delta^{15}N_{\text{diamond – fluid}}$ = -4.0) through Petts et al. (2015) now allows to add $\delta^{15}N$ as an additional parameter to models simulating the formation of diamond in fluid limited systems. As stated above, nitrogen-in-diamond based thermometry indicates that about 80% of the studied Chidliak diamonds grew within ±50 °C of the temperature for which Petts et al. (2015) derived their isotope fractionation factor, allowing for application of this value without temperature corrections. In addition, like the majority of Chidliak diamonds, the sample studied by Petts et al. (2015) formed in an eclogitic substrate. The studies of Li and Keppler (2014) and Mikhail and Sverjensky (2014) predict that for diamond formation in the deep lithospheric mantle only a single dominant nitrogen species has to be considered. Despite the unresolved exact nature of this nitrogen species (either NH_3 or NH_4^+), the absence of predicted speciation changes across the fO_2 range of typical diamond forming conditions suggests that the fractionation factor of Petts et al. (2015) should be widely applicable. Figure 10 shows that due to the small absolute value of $\Delta^{13}C_{\text{diamond - fluid}}$ relative to $\Delta^{15}N_{\text{diamond – fluid}}$, $\delta^{13}C$ is insensitive to moderate amounts of Rayleigh fractionation when

compared to $\delta^{15}N$. For example, 50% diamond crystallization from a carbonatitic fluid would lead to an increase of 12.2 ‰ in $\delta^{15}N$ but only of 1.2 ‰ in $\delta^{13}C$. With this background it is not surprising that no coherent trends involving $\delta^{13}C$ are observed in Figure 5 (with [N]) and Figure 10 (with $\delta^{15}N$), whereas extended linear arrays are apparent when co-variations between $\delta^{15}N$ and [N] are considered (Fig. 8). The observed large variability in the carbon isotopic composition of CH-6 and CH-7 diamonds (from mantle-like compositions to $\delta^{13}C$ as low as -28.4 ‰), therefore, is not interpreted as a product of isotopic fractionation but rather as a consequence of the contribution of subducted, organic matter-derived carbon to a diamond suite that mostly grew from mantle carbon (see section 4.2.1). Consequently, only co-variations between $\delta^{15}N$ and [N] are considered for the testing of a Rayleigh fractionation hypothesis.

Figure 8 shows Rayleigh fractionation trends calculated using the values for $\Delta^{15}N_{diamond-fluid}$ and K_N, derived by Petts et al. (2015; see above) and the equation for N-isotope fractionation described by Cartigny et al. (2001). The calculated trends perfectly match the linear arrays visible in the data set (Fig. 8) without requiring excessively high degrees of fractionation (both arrays require about 60% crystallization). The Rayleigh fractionation trends also match the internal variations seen in some CH-6 and CH-7 diamonds (Fig. 7B). To test the sensitivity of our model to the choice of K_N=4.4 (Petts et al., 2015), we modelled the trends depicted in Figure 8 using the highest (K_N=5, Smart et al., 2011) and lowest (K_N=2, Thomassot et al., 2007) published values for lithospheric diamonds. Using a K_N of 5 has no significant effect, the modelled nitrogen isotope factor increases from 4.0 to 4 .2. Using a K_N of 2, however, decreases the nitrogen fractionation factor to -2.6 and, as a corollary, predicts that the observed trends in $\delta^{15}N$–[N] should be associated with significant co-variations in $\delta^{13}C$. Assuming diamond precipitation from a carbonate melt ($\Delta^{13}C_{diamond-fluid}$ = -1.7, see above), the internal variations in $\delta^{15}N$ of about 5 ‰ seen for a number of samples in Figure 11 then would need to be associated with an increase in $\delta^{13}C$ of about 1.6 ‰. For the majority of samples (Fig. 11), internal variations in $\delta^{13}C$ are within or near analytical error, consistent with the 0.5 ‰ variation in $\delta^{13}C$ predicted over the same interval using the Petts et al. (2015) parameters for nitrogen partitioning and isotope fractionation. This affirms that the K_N and $\Delta^{15}N_{diamond-fluid}$ values of Petts et al. (2015) are an appropriate choice for modelling Chidliak diamond compositional trends.

The large variability of nitrogen contents in diamonds with mantle-like $\delta^{15}N$ and the apparent presence of two starting compositions with slightly distinct $\delta^{15}N$ (and distinct [N]) are

interpreted to represent variability in the composition of the original diamond forming fluid. This variability leads to a broadening of the two observed fractionation trends and the possible presence of additional shorter arrays. The subset of samples with $\delta^{13}C$ between -10 and -20 ‰ appears to fall on the same linear arrays as the group with mantle-like carbon (Fig. 8). Viewed in isolation, however, this moderately ^{13}C depleted group shows no clear co-variations between $\delta^{15}N$ and [N], but large variability of nitrogen content at generally positive $\delta^{15}N$ instead. Internal variations in $\delta^{15}N$–[N] in diamonds CH6-6 and CH6-38 (Fig. 7B) are consistent with the calculated Rayleigh fractionation trends though. To relate the absence of clear inter-sample fractionation trends within the moderately ^{13}C depleted group to the comparatively small number of samples, therefore, appears the simplest explanation. It cannot be established if the Rayleigh fractionation model can solely be employed to explain the $\delta^{15}N$–[N] variations seen for strongly ^{13}C depleted diamonds ($\delta^{13}C$ <-20 ‰; Fig. 8). Rather than a linear array, these samples form two clusters in $\delta^{15}N$–log[N] space and, therefore, could equally represent a subducted ^{13}C-depleted component with low nitrogen content and positive $\delta^{15}N$ that only for some samples experienced addition of mantle derived N (with negative $\delta^{15}N$).

For diamonds with mantle-like $\delta^{13}C$, however, the presence of linear trends clearly documents nitrogen fractionation during diamond precipitation in a fluid limited system. This finding is inconsistent with a decoupling of carbon and nitrogen isotope systematics in diamond (Mikhail et al., 2014). At least for the diamond suite studied, the apparent decoupling relates to a much higher isotopic fractionation factor for nitrogen compared to carbon during diamond growth, leading to variations in $\delta^{15}N$ that are one order of magnitude higher than those in $\delta^{13}C$. This is prominently depicted when looking at internal compositional variations of CH-6 and CH-7 diamonds, where large fluctuations in $\delta^{15}N$ from growth zone to growth zone occur at nearly constant $\delta^{13}C$ (Fig. 11).

5.0 Conclusions

A combination of CL imaging and SIMS microbeam analyses reveals that Chidliak diamond growth was complex, with at least two separate (with a stage of diamond resorption in between) diamond growth events with distinct carbon isotope signatures and nitrogen contents. Multiple fluid pulses likely account for fluctuations in $\delta^{13}C$–[N] across consecutive growth zones. The

$\delta^{13}C$ distribution and overall high nitrogen contents of the studied diamond suite are consistent with a predominantly eclogitic paragenesis, which is validated by an exclusive correlation between eclogitic indicator mineral counts and diamond content in Chidliak kimberlite samples.

The interrelationship of $\delta^{13}C$, nitrogen content and $\delta^{15}N$ for CH-6 and CH-7 diamonds appears extremely complex. Nevertheless, by taking the one order of magnitude higher sensitivity of $\delta^{15}N$ relative to $\delta^{13}C$ to isotopic fractionation during diamond growth from a fluid into account, the complexity can be understood as reflecting three main processes: (1.) the presence or introduction of subducted (organic matter-derived) carbon in the source rocks of some Chidliak diamonds establishes a ^{13}C depleted reservoir. Judging from diamonds that show a major growth hiatus, early growth dominated by this subducted carbon component was associated with relatively low nitrogen contents. (2.) A fluid with approximately mantle-like $\delta^{13}C$ and $\delta^{15}N$ but variable nitrogen content repeatedly infiltrated diamond substrates in the lithospheric mantle and caused precipitation of this diamond suite. During these events, any graphitized organic matter present in the diamond source rocks likely was re-mobilized in a dissolution and re-precipitation process. Only the organic matter-enriched topmost portion of altered basaltic seafloor provides a protolith for eclogitic substrates that during later fluid influx and diamond formation retains a distinctly ^{13}C depleted signature, whilst in deeper levels of subducted oceanic crust diamond carbon is completely dominated by the fluid composition (Ickert et al., 2013). (3.) During diamond precipitation the availability of fluid became occasionally limited and Rayleigh isotope fractionation occurred in these instances, creating at least two compositional arrays reflecting large co-variation in $\delta^{15}N$–log[N] at nearly constant $\delta^{13}C$. We suggest that the last process, reflecting the much higher sensitivity of $\delta^{15}N$ and [N] (relative to $\delta^{13}C$) to fractionation processes, is the true cause of an apparent decoupling of $\delta^{15}N$ and $\delta^{13}C$ observed for diamonds world-wide. This conclusion also implies that, in isolation, positive $\delta^{15}N$ values cannot be employed as a faithful indicator of subduction-related nitrogen in diamond.

Acknowledgements

Peregrine Diamonds Ltd. is thanked for the donation of the diamonds for this study, and for the

permission to publish the data. Jennifer Pell, Herman Grütter (both Peregrine Diamonds), Tom McCandless, Jeff Harris and Tom Chacko provided valuable input at various stages of the project. David Mate and Rosemarie Kuhn (then Canada-Nunavut Geoscience Office) are thanked for enthusiastically supporting this project. We also thank Sami Mikhail, Pierre Cartigny, and an anonymous reviewer for their comments on this manuscript, which greatly improved it. Fabrizio Nestola is thanked for his editorial work. K.H. gratefully acknowledges a Research Affiliate Program (RAP) bursary through Natural Resources Canada and additional financial support through the Canada-Nunavut Geoscience Office. T.S. acknowledges research funding through an NSERC Discovery Grant and additional support through the Canada Research Chairs Program.

References

Bebout, G.E., Fogel, M.L., 1992. Nitrogen-isotope compositions of metasedimentary rocks in the Catalina Schist, California: Implications for metamorphic devolatilization history. Geochimica et Cosmochimica Acta, 56(7): 2839-2849.

Bottinga, Y., 1969. Calculated fractionation factors for carbon and hydrogen isotope exchange in the system calcite-carbon dioxide-graphite-methane-hydrogen-water vapor. Geochimica et Cosmochimica Acta 33, 49-64.

Boyd, S.R., Pineau, F., Javoy, M., 1994. Modelling the growth of natural diamonds. Chemical Geology, 116, 29-42.

Bulanova, G.P., Pearson, D.G., Hauri, E.H., Griffin, B.J., 2002. Carbon and nitrogen isotope systematics within a sector-growth diamond from the Mir kimberlite, Yakutia. Chemical Geology, 188, 105-123

Bulanova, G.P., Wiggers de Vries, D.F., Pearson, D.G., Beard, A., Mikhail, S., Smelov, A.P., Davies, G.R., 2014. An eclogitic diamond from Mir pipe (Yakutia), recording two growth events from different isotopic sources. Chemical Geology, 381(0), 40-54.

Busigny, V., Bebout, G.E., 2013. Nitrogen in the silicate earth: Speciation and isotopic behavior during mineral-fluid interactions. Elements, 9(5): 353-358.

Busigny, V., Cartigny, P., Philippot, P., Ader, M., Javoy, M., 2003. Massive recycling of nitrogen and other fluid-mobile elements (K, Rb, Cs, H) in a cold slab environment: Evidence from HP to UHP oceanic metasediments of the Schistes Lustrés nappe (western

Alps, Europe). Earth and Planetary Science Letters, 215(1-2): 27-42.

Cartigny, P., 2005. Stable isotopes and the origin of diamond. Elements, 1(2): 79-84.

Cartigny, P., Harris, J.W., Javoy, M., 1998. Eclogitic diamond formation at Jwaneng: No room for a recycled component. Science, 280(5368): 1421-1424.

Cartigny, P., Harris, J.W., Javoy, M., 2001. Diamond genesis, mantle fractionations and mantle nitrogen content: A study of $\delta^{13}C$ Diamond Carbon isotopes-N concentrations in diamonds. Earth and Planetary Science Letters, 185(1-2): 85-98.

Cartigny, P., Jendrzejewski, N., Pineau, F., Petit, E., Javoy, M., 2001b. Volatile (C, N, Ar) variability in MORB and the respective roles of mantle source heterogeneity and degassing: The case of the Southwest Indian Ridge. Earth and Planetary Science Letters, 194(1-2): 241-257.

Cartigny, P., Marty, B., 2013. Nitrogen isotopes and mantle geodynamics: The emergence of life and the atmosphere-crust-mantle connection. Elements, 9(5): 359-366.

Cartigny, P., Palot, M., Thomassot, E., Harris, J.W., 2014. Diamond Formation: A Stable Isotope Perspective. Annual Review of Earth and Planetary Sciences, 42(1), 699-732.

Chacko, T., Mayeda, T.K., Clayton, R.N., Goldsmith, J.R., 1991. Oxygen and carbon isotope fractionations between CO_2 and calcite. Geochimica et Cosmochimica Acta, 55(10): 2867-2882.

De Stefano, A., Kopylova, M.G., Cartigny, P., Afanasiev, V., 2009. Diamonds and eclogites of the Jericho kimberlite (Northern Canada). Contributions to Mineralogy and Petrology, 158(3), 295-315.

Deines, P., 2002. The carbon isotope geochemistry of mantle xenoliths. Earth Science Reviews, 58(2002), 247-278.Deines, P., 1980. The carbon isotopic composition of diamonds: relationship to diamond shape, color, occurrence and vapor composition. Geochimica et Cosmochimica Acta, 44(7): 943-961.

Deines, P., Harris, J.W., Gurney, J.J., 1993. Depth-related carbon-isotope and nitrogen concentration variability in the mantle below the Orapa kimberlite, Botswana, Africa. Geochimica et Cosmochimica Acta, 57(12): 2781-2796.

Deines, P., Gurney, J.J., Harris, J.W., 1984. Associated chemical and carbon isotopic composition variations in diamonds from Finsch and Premier kimberlite, South Africa. Geochimica et Cosmochimica Acta, 48(2): 325-342.

Duit, W., Jansen, J.B.H., Van Breemen, A., Bos, A., 1986. Ammonium micas in metamorphic rocks as exemplified by Dome de l'Agout (France). American Journal of Science, 286(9): 702-732.

Faure, G., 1986. Principles of Isotope Geology. Wiley, 589 pp

Fischer, T.P., Takahata, N., Sano, Y., Sumino, H., Hilton, D.R., 2005. Nitrogen isotopes of the mantle: Insights from mineral separates. Geophysical Research Letters, 32(11): L11305.

Grütter, H.S., Gurney, J.J., Menzies, A.H., Winter, F., 2004. An updated classification scheme for mantle-derived garnet, for use by diamond explorers. Lithos 77, 841-857.

Haendel, D., Mühle, K., Nitzsche, H.-M., Stiehl, G., Wand, U., 1986. Isotopic variations of the fixed nitrogen in metamorphic rocks. Geochimica et Cosmochimica Acta 50, 749-758.

Hauri, E.H., Wang, J., Pearson, D.G., Bulanova, G.P., 2002. Microanalysis of $\delta^{13}C$, $\delta^{15}N$, and N abundances in diamonds by secondary ion mass spectrometry. Chemical Geology, 185(1-2): 149-163.

Ickert, R.B., Stachel, T., Stern, R.A., Harris, J.W., 2013. Diamond from recycled crustal carbon documented by coupled $\delta^{18}O$-$\delta^{13}C$ measurements of diamonds and their inclusions. Earth and Planetary Science Letters, 364: 85-97.

Ickert, R.B., Stachel, T., Stern, R.A., Harris, J.W., 2015. Extreme 18O-enrichment in majorite constrains a crustal origin of transition zone diamonds. Geochemical Perspectives Letters, 1(0), 65-74.

Kirkley, M.B., Gurney, J.J., Otter, M.L., Hill, S.J., Daniels, L.R., 1991. The application of C isotope measurements to the identification of the sources of C in diamonds: a review. Applied Geochemistry, 6(5): 477-494.

Javoy, M., 1997. The major volatile elements of the Earth: Their origin, behavior, and fate. Geophysical Research Letters 24(2): 177-180.

Javoy, M., Pineau, F., Delorme, H., 1986. Carbon and nitrogen isotopes in the mantle. Chemical Geology, 57(1-2): 41-62.

Johnson, B., Goldblatt, C., 2015. The nitrogen budget of Earth. Earth-Science Reviews, 150.

Lang, A.R., 1979. Internal Structure. In: J.E. Field (Editor), The Properties of Diamond. Academic Press, London, pp. 425-469.

Li, L., Bebout, G.E., Idleman, B.D., 2007. Nitrogen concentration and δ15N of altered oceanic crust obtained on ODP Legs 129 and 185: Insights into alteration-related nitrogen

enrichment and the nitrogen subduction budget. Geochimica et Cosmochimica Acta, 71(9): 2344-2360.

Li, Y., Keppler, H., 2014. Nitrogen speciation in mantle and crustal fluids. Geochimica et Cosmochimica Acta, 129: 13-32.

Ludwig, K.R., 1999. Using Isoplot/Ex, Version 2.01: a geochronological toolkit for Microsoft Excel. Berkeley Geochronology Center Special Publication, 1a, 47.

Mariotti, A., Landreau, A., Simon, B., 1988. 15N isotope biogeochemistry and natural denitrification process in groundwater: Application to the chalk aquifer of northern France. Geochimica et Cosmochimica Acta, 52(7), 1869-1878.

Martin, J.M.L., Lee, T.J., 1996. Accurate ab initio quartic force field and vibrational frequencies of the NH4+ ion and its deuterated forms. Chemical Physics Letters 258, 129-135.

Martin, J.M.L., Lee, T.J., Taylor, P.R., 1992. An accurate ab initio quartic force field for ammonia. The Journal of Chemical Physics 97, 8361-8371.

Marty, B., 1995. Nitrogen content of the mantle inferred from N2-Ar correlation in oceanic basalts. Nature, 377(6547): 326-329.

Marty, B., Dauphas, N., 2003. The nitrogen record of crust–mantle interaction and mantle convection from Archean to Present. Earth and Planetary Science Letters, 206(3–4): 397-410.

McCandless, T.E., Gurney, J.J., 1997. Diamond eclogites: Comparison with carbonaceous chondrites, carbonaceous shales, and microbial carbon-enriched more. Geologiya i Geofizika, 38(2): 371-381.

Mikhail, S., Howell, D., 2016. A petrological assessment of diamond as a recorder of the mantle nitrogen cycle. American Mineralogist, 101(4), 780-787.

Mikhail, S., Sverjensky, D.A., 2014. Nitrogen speciation in upper mantle fluids and the origin of Earth's nitrogen-rich atmosphere. Nature Geoscience, 7(11), 816-819.

Mikhail, S., Guillermier, C., Franchi, I.A., Beard, A.D., Crispin, K., Verchovsky, A.B., Jones, A.P., Milledge, H.J., 2014. Empirical evidence for the fractionation of carbon isotopes between diamond and iron carbide from the Earth's mantle. Geochemistry Geophysics Geosystems, 15(4), 855-866.

Mikhail, S., Verchovsky, A.B., Howell, D., Hutchison, M.T., Southworth, R., Thomson, A.R., Warburton, P., Jones, A.P., Milledge, H.J., 2014. Constraining the internal variability of

the stable isotopes of carbon and nitrogen within mantle diamonds. Chemical Geology, 366: 14-23.

Milledge, H.J., Mendelssohn, M.J., Seal, M., Rouse, J.E., Swart, P.K., Pillinger, C.T., 1983. Carbon isotopic variation in spectral Type II diamonds. Nature, 303(5920): 791-792.

Nadeau, S., Pineau, F., Javoy, M., Francis, D., 1990. Carbon concentrations and isotopic ratios in fluid-inclusion-bearing upper-mantle xenoliths along the northwestern margin of North America. Chemical Geology, 81(4): 271-297.

Navon, O., Hutcheon, I.D., Rossman, G.R., Wasserburg, G.J., 1988. Mantle-derived fluids in diamond micro-inclusions. Nature, 335(6193), 784-789.

Neilson, S, G.H., Pell. J., Grenon. H, 2012. The Evolution of Kimberlite Indicator Mineral Interpretation on the Chidliak Project, Baffin Island, Nunavut. 10th International Kimberlite Conference, Bangalore, conference CD (abstract 162).

Nichols, K.M.A., 2014. Diamond sources beneath the Hall Peninsula, Baffin Island, Nunavut: A preliminary assessment based on Chidliak diamonds. MSc Thesis, Education and Research Archives, University of Alberta.

Palot, M., Pearson, D.G., Stern, R.A., Stachel, T., Harris, J.W., 2013. Multiple growth events, processes and fluid sources involved in diamond genesis; a micro-analytical study of sulphide-bearing diamonds from Finsch Mine, RSA. Geochimica et Cosmochimica Acta 106, 51-70.

Palot, M., Pearson, D.G., Stern, R.A., Stachel, T., Harris, J.W., 2014. Isotopic constraints on the nature and circulation of deep mantle C–H–O–N fluids: Carbon and nitrogen systematics within ultra-deep diamonds from Kankan (Guinea). Geochimica Et Cosmochimica Acta, 139(0), 26-46.

Pell, J., Farrow, D., 2012. Updated 2011 Technical report on the Chidliak Property, Baffin Region, Nunavut; Peregrine Diamonds 148 unpublished report Updated 2011 Technical report on the Chidliak Property, Baffin Region, Nunavut; Peregrine Diamonds.

Pell, J., Grütter, H., Dempsey, S., Neilson, S., 2012. Exploration and discovery of the Chidliak kimberlite province, Baffin Island, Nunavut: Canada's newest diamond district. 10th International Kimberlite Conference, Bangalore, conference CD (abstract 40).

Pell, J., Grütter, H., Neilson, S., Lockhart, G., Dempsey, S., Grenon, H., 2013. Exploration and Discovery of the Chidliak Kimberlite Province, Baffin Island, Nunavut: Canada's Newest

Diamond District. In: D.G. Pearson, H.S. Grütter, J.W. Harris, B.A. Kjarsgaard, H. O'Brien, N.V.C. Rao and S. Sparks (Editors), Proceedings of 10th International Kimberlite Conference. Springer India, Bangalore, India. 209-227.

Peters, K.E., Sweeney, R.E., Kaplan, I.R., 1978. Correlation of Carbon and Nitrogen Stable Isotope Ratios in Sedimentary Organic Matter. Limnology and Oceanography, 23(4): 598-604.

Petts, D.C., Chacko, T., Stachel, T., Stern, R.A., Heaman, L.M. (2015) A nitrogen isotope fractionation factor between diamond and its parental fluid derived from detailed SIMS analysis of a gem diamond and theoretical calculations. Chemical Geology, 410: 188-200.

Reutsky, V.N., Borzdov, Y.M., Palyanov, Y.N., 2008. Carbon isotope fractionation associated with HPHT crystallization of diamond. Diamond & Related Materials 17, 1986-1989.

Richet, P., Bottinga, Y., Javoy, M., 1977. Review of hydrogen, carbon, nitrogen, oxygen, sulfur, and chlorine stable isotope fractionation among gaseous molecules. Annual Review of Earth and Planetary Sciences 5, 65-110.

Rondeau, B., Fritsch, E., Guiraud, M., Chalain, J.P., Notari, F., 2004. Three historical 'asteriated' hydrogen-rich diamonds: Growth history and sector-dependent impurity incorporation. Diamond and Related Materials, 13(9): 1658-1673.

Sellschop, J.P.F., Madiba, C.C.P., Annegarn, H.J., 1980. Light volatiles in diamond: Physical interpretation and genetic significance. Nuclear Instruments and Methods, 168(1–3): 529-534.

Shilobreeva, S., Martinez, I., Busigny, V., Agrinier, P., Laverne, C., 2011. Insights into C and H storage in the altered oceanic crust: Results from ODP/IODP Hole 1256D. Geochimica et Cosmochimica Acta, 75(9): 2237-2255.

Schulze, D.J., Harte, B., Valley, J.W., Brenan, J.M., Channer, D.M.D., 2003. Extreme crustal oxygen isotope signatures preserved in coesite in diamond. Nature, 423(6935), 68-70.

Schulze, D.J., Harte, B., Page, F.Z., Valley, J.W., Channer, D.M.D., Jaques, A.L., Edinburgh Ion Microprobe Facility, 2013. Anticorrelation between low $\delta^{13}C$ of eclogitic diamonds and high $\delta^{18}O$ of their coesite and garnet inclusions requires a subduction origin. Geology, 41(4), 455-458.

Smart, K.A., Chacko, T., Stachel, T., Muehlenbachs, K., Stern, R.A., Heaman, L.M., 2011.

Diamond growth from oxidized carbon sources beneath the Northern Slave Craton, Canada: A δ13C–N study of eclogite-hosted diamonds from the Jericho kimberlite. Geochimica et Cosmochimica Acta, 75(20): 6027-6047.

Stachel, T., 2014. Diamond. Mineralogical Association of Canada Short Course Series, 44, 1-28.

Stachel, T., Luth, R.W., 2015. Diamond formation — Where, when and how? Lithos, 220–223, 200-220.

Stachel, T., Harris, J.W., 1997. Syngenetic inclusions in diamond from the Birim field (Ghana) - A deep peridotitic profile with a history of depletion and re-enrichment. Contributions to Mineralogy and Petrology, 127(4): 336-352.

Stachel, T., Harris, J.W., 2008. The origin of cratonic diamonds - Constraints from mineral inclusions. Ore Geology Reviews, 34(1-2): 5-32.

Stachel, T., Harris, J.W., 2009. Formation of diamond in the Earth's mantle. Journal of Physics - Condensed Matter, 21(36).

Stachel, T., Harris, J.W., Muehlenbachs, K., 2009. Sources of carbon in inclusion bearing diamonds. Lithos, 112: 625-637.

Sobolev, V.S., Sobolev, N.V., 1980. New proof on very deep subsidence of eclogitized crustal rocks. Doklady Akademii Nauk SSSR, 250(3): 683-685.

Taylor, L.A., Milledge, H.J., Bulanova, G.P., Snyder, G.A., Keller, R.A., 1998. Metasomatic eclogitic diamond growth: Evidence from multiple diamond inclusions. International Geology Review, 40(8), 663-676.

Tappert, R., Stachel, T., Harris, J.W., Muehlenbachs, K., Ludwig, T., Brey, G.P., 2005. Subducting oceanic crust: The source of deep diamonds. Geology, 33(7), 565-568.

Thomassot, E., Cartigny, P., Harris, J.W., Viljoen, K.S., 2007. Methane-related diamond crystallization in the Earth's mantle: Stable isotope evidences from a single diamond-bearing xenolith. Earth and Planetary Science Letters, 257(3-4): 362-371.

Thomazo, C., Papineau, D., 2013. Biogeochemical cycling of nitrogen on the early earth. Elements, 9(5): 345-351.

Watenphul, A., Wunder, B., Heinrich, W., 2009. High-pressure ammonium-bearing silicates: Implications for nitrogen and hydrogen storage in the Earth's mantle. American Mineralogist, 94(2-3): 283-292.

Watenphul, A., Wunder, B., Wirth, R., Heinrich, W., 2010. Ammonium-bearing clinopyroxene:

A potential nitrogen reservoir in the Earth's mantle. Chemical Geology, 270(1-4): 240-248.

Weiss, Y., Kiflawi, I., Davies, N., Navon, O., 2014. High-density fluids and the growth of monocrystalline diamonds. Geochimica et Cosmochimica Acta, 141(0), 145-159.

Wiggers de Vries, D.F., Bulanova, G.P., De Corte, K., Pearson, D.G., Craven, J.A., Davies, G.R., 2013. Micron-scale coupled carbon isotope and nitrogen abundance variations in diamonds: Evidence for episodic diamond formation beneath the Siberian Craton. Geochimica et Cosmochimica Acta, 100(0), 176-199.

Wilks, J., Wilks, E., 1991. Properties and applications of diamond. Butterworth-Heinemann, Oxford, UK, 525 pp.

Wyllie, P.J., Huang, W.-L., 1976. Carbonation and melting reactions in the system CaO-MgO-SiO2-CO2 at mantle pressures with geophysical and petrological applications. Contributions to Mineralogy and Petrology, 54, 79-107.

Yokochi, R., Marty, B., Chazot, G., Burnard, P., 2009. Nitrogen in peridotite xenoliths: Lithophile behavior and magmatic isotope fractionation. Geochimica Et Cosmochimica Acta, 73(16), 4843-4861.

Zedgenizov, D.A., Harte, B., EIMF, Shatsky, V.S., Politov, A.A., Rylov, G.M., Sobolev, N.V., 2006. Directional chemical variations in diamonds showing octahedral following cuboid growth. Contributions to Mineralogy and Petrology, 151(1), 45-57.

Figure and Table Captions

Table 1. $\delta^{13}C$, $\delta^{15}N$ and nitrogen contents measured via SIMS for 94 Chidliak diamonds. N_C and N_N are nitrogen contents (at.ppm) determined on the adjacent analytical spots employed for the analysis of $\delta^{13}C$ and $\delta^{15}N$, respectively. Analtical uncertainties (2 sigma) for carbon and nitrogen isotope analyses reflect external reproducibility. The various types of CL patterns are defined in section 4.1.

Fig. 1. Distribution of $\delta^{13}C$ values for CH-6 and CH-7 diamonds (A; multiple point analyses per diamond are shown; the red line is a probability density curve calculated using Isoplot; Ludwig, 1999) compared to eclogitic diamonds from deposits elsewhere in Canada (B), eclogitic and

websteritic diamonds worldwide (C), and peridotitic diamonds worldwide (D; B-D are bulk analyses from the database of Stachel et al., 2009). Eclogitic diamonds from the Jericho kimberlite were excluded from the Canadian data set as their in part extremely negative carbon isotopic compositions (as low as -41.4 ‰; De Stefano et al. 2009), suggestive of bacterial methane fixation in a sedimentary protolith (Smart et al., 2011), are unique worldwide.

Fig. 2. A: Averaged nitrogen contents (at.ppm; based on the analytical data derived on the $\delta^{13}C$ spot locations) of individual CH-6 and CH-7 diamonds compared to eclogitic-websteritic (B) and peridotitic diamonds (C) from worldwide sources (FTIR bulk analyses; database of Stachel et al., 2009). CH-6 and CH-7 diamonds have a bimodal distribution similar to eclogitic diamonds worldwide, with the second mode being shifted to higher concentrations (from class 400-600 to class 1000-1200 at.ppm). The median nitrogen content of the combined Chidliak sample suite is 1112 at.ppm, compared to 489 at.ppm for eclogitic and 86 at.ppm for peridotitic diamonds worldwide.

Fig. 3. A: $\delta^{15}N$ values of CH-6 and CH-7 diamonds measured via SIMS; nitrogen isotopic compositions are not averaged (i.e., multiple measurements are reported for each diamond). The red line is a probability density curve. For comparison, $\delta^{15}N$ values for worldwide eclogitic (B) and peridotitic (C) diamonds are also shown (bulk analyses, for references see Stachel et al., 2009).

Fig. 4. Annotated CL images. Spot size for SIMS analyses is approximately 15 µm (represented by open circles); for each spot $\delta^{13}C$ (‰) is given above the nitrogen content (N_C; at.ppm) followed by the italicised value for $\delta^{15}N$ (‰), where applicable. A: diamond CH6-46 is likely a re-entrant cube, exhibiting a "hiatus" from very dark CL to lighter banded CL. An abrupt change of $\delta^{13}C$ and nitrogen content is observed across the hiatus, which appears to represent a resorption front. B: CH7-23 is an example of homogeneous CL; $\delta^{13}C$ values and nitrogen content are consistent across the diamond. C: CH6-32 demonstrates both agate-like banding and octahedral (perfectly planar) growth; distinct variations in $\delta^{13}C$, nitrogen content and $\delta^{15}N$ are observed. D: CH6-45 shows cuboid growth and is also an aggregate, with two dark central areas likely representing two initial growth centres; again significant changes in $\delta^{13}C$, nitrogen content and $\delta^{15}N$ are associated with changes in the CL response. E and F: CH6-3 and CH6-21 exhibit complex internal growth structures. CH6-3 shows a "centre-cross pattern" reflecting mixed habit (cuboid and octahedral) growth (e.g., Rondeau et al., 2004). CH6-21 is “complex” and possibly demonstrates the CL response of platelets (Lang, 1979) oriented along octahedral planes.

Fig. 5. Nitrogen content and carbon isotopic composition of CH-6 and CH-7 diamonds measured via SIMS; error of $\delta^{13}C$ analyses is smaller than the symbol size.

Fig. 6. $\delta^{15}N$ versus $\delta^{13}C$ for CH-6 and CH-7 diamonds. Error of $\delta^{13}C$ analyses is smaller than the symbol size, error bars for $\delta^{15}N$ are 2 sigma. Individual spot analyses are shown for each diamond.

Fig. 7. A: Plot of total nitrogen content (N_N; log scale) against $\delta^{15}N$. Diamonds from kimberlite CH-7 (blue squares) mostly cluster around the mantle value for $\delta^{15}N$ (about -5 ‰), while diamonds from kimberlite CH-6 (green triangles) show overall more variability. Subparallel trends of decreasing N content with increasing $\delta^{15}N$ extend to strongly positive $\delta^{15}N$ values. Individual spot analyses are shown for each diamond. B: Multiple spot analyses of diamonds showing significant internal variations in N content and $\delta^{15}N$. The sub-parallel trends of decreasing nitrogen content with increasing $\delta^{15}N$ (Fig. 7A) clearly persist on the level of individual diamonds, although not in the form of systematic core-rim variations. Samples are grouped according to mantle-like ($\delta^{13}C$ between -1 to -10 ‰; closed symbols) and moderately ^{13}C-depleted ($\delta^{13}C$ between -10 to -20 ‰; open symbols) carbon isotopic compositions.

Fig. 8. Plot of nitrogen content (N_N; log scale) versus $\delta^{15}N$ (‰), with samples being grouped according to their carbon isotopic composition. Considering only samples with mantle like $\delta^{13}C$ (-10 to -1 ‰), two linear arrays from high N and low $\delta^{15}N$ towards low N and high $\delta^{15}N$ are evident. The black dashed arrows are calculated Rayleigh fractionation trends, based on the N-isotope fractionation factor ($\Delta^{15}N_{\text{diamond - fluid}} = -4.0$) and the diamond-fluid nitrogen partition coefficient ($K_N = 4.4$) derived by Petts et al. (2015). The initial diamond composition and the composition at 50% residual fluid (f=0.5) are indicated as open circles. Analyses with mantle-like $\delta^{13}C$ that fall into the field outlined with a pink dotted line constitute the "higher nitrogen trend" and are isolated in Figure 9.

Fig. 9. Reciprocal nitrogen content versus $\delta^{15}N$ for samples with mantle like $\delta^{13}C$ constituting the "higher nitrogen trend" in Figure 8. The data points are best fitted by an exponential trend-line (dashed black line), implying that the relationship between nitrogen content and $\delta^{15}N$ is caused by Rayleigh fractionation rather than binary mixing.

Fig. 10. Carbon versus nitrogen isotopic composition of CH-6 and CH-7 diamonds. Symbols are assigned according to a subdivision of analytical spot locations into five groups, ranging from very nitrogen rich (>3000 at.ppm) to nitrogen poor (<100 at.ppm). Using the isotopic fractionation factors discussed in the text, Rayleigh fractionation trends involving three diamond-forming carbon species (CO_2, $CaCO_3$, and CH_4) are shown. The initial diamond composition and the composition at 50% crystallization (f=0.5) are indicated as open circles. Note that in more dilute fluids (e.g. water-bearing fluids) the degree of fractionation required would decrease (see main text). For all three possible carbon species, $\delta^{15}N$ clearly is a much more sensitive recorder of Rayleigh fractionation processes during diamond formation than $\delta^{13}C$.

Fig. 11. Variations of $\delta^{15}N$ and $\delta^{13}C$ within individual diamonds exhibiting the sub-parallel trends of decreasing nitrogen content with increasing $\delta^{15}N$. Errors of $\delta^{13}C$ analyses are smaller than the symbol size, errors shown for $\delta^{15}N$ are 2 sigma. Large internal variations in $\delta^{15}N$ occur at $\delta^{13}C$ values that generally are constant within analytical uncertainty.

Figure 1

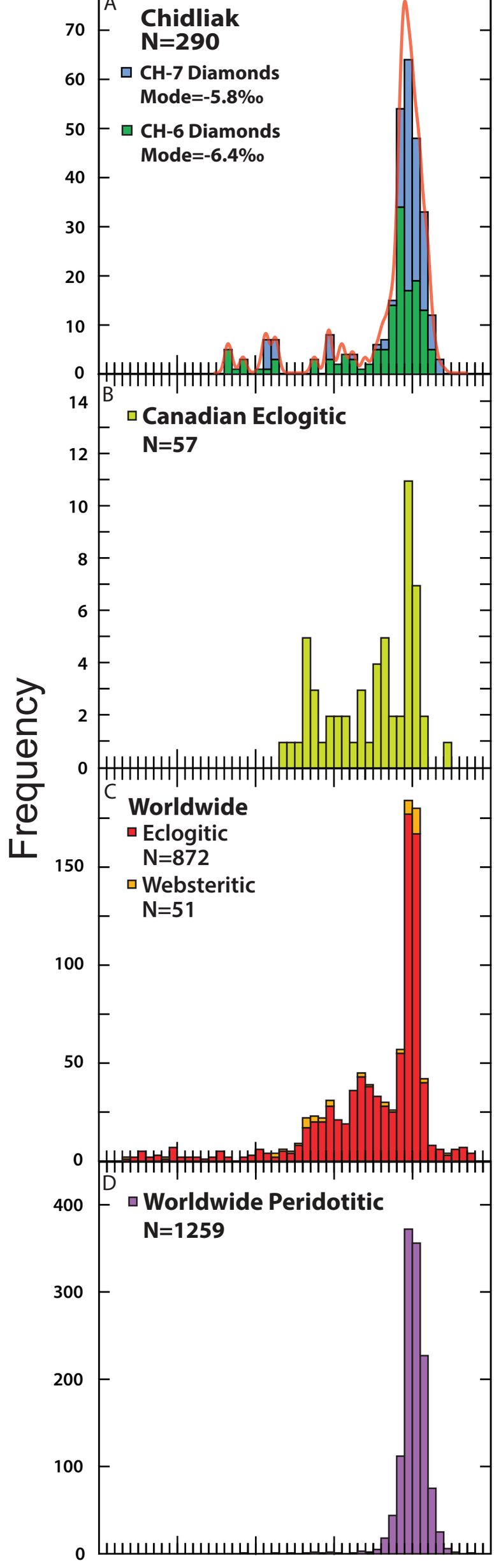
A
Chidliak
N=290
CH-7 Diamonds
Mode=-5.8‰
CH-6 Diamonds
Mode=-6.4‰
B
Canadian Eclogitic
N=57
C
Worldwide
Eclogitic
N=872
Websteritic
N=51
D
Worldwide Peridotitic
N=1259
Frequency

Figure 2

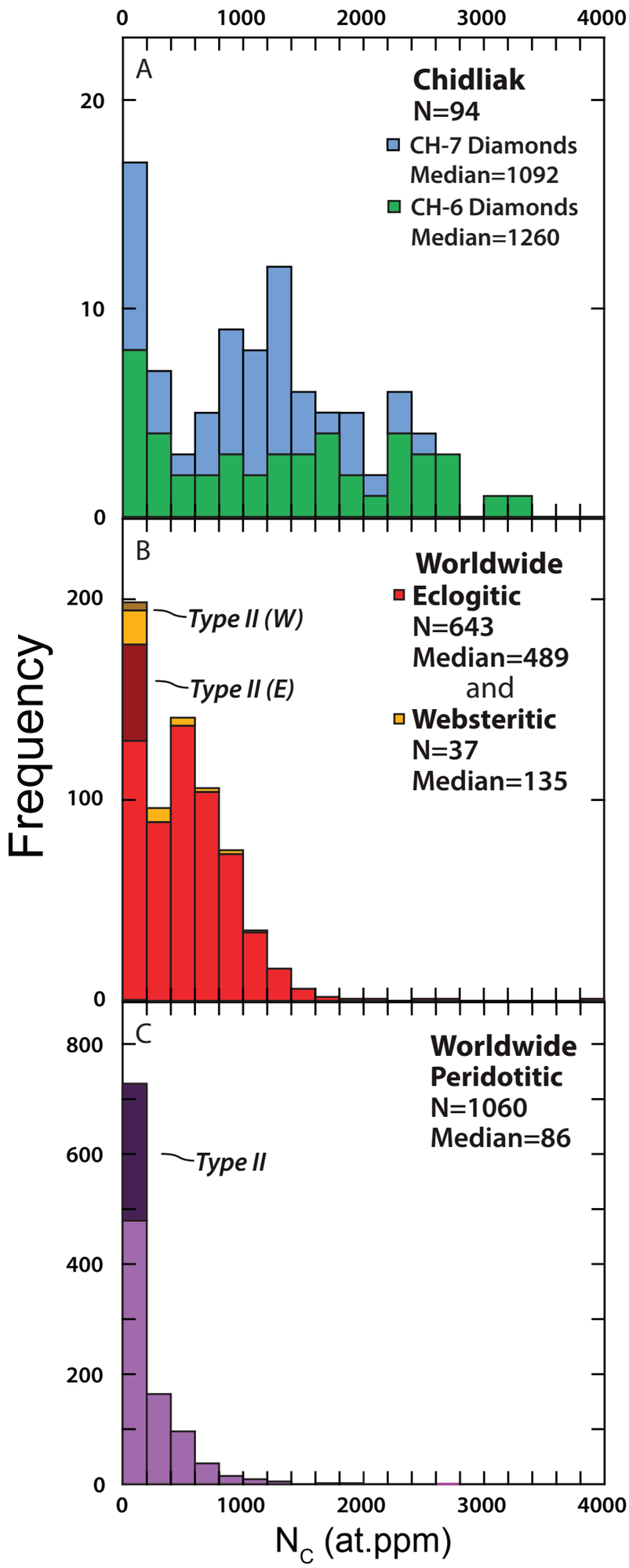
A
Chidliak
N=94
CH-7 Diamonds
Median=1092
CH-6 Diamonds
Median=1260
B
Worldwide
Eclogitic
N=643
Median=489
and
Websteritic
N=37
Median=135
Type II (W)
Type II (E)
C
Worldwide
Peridotitic
N=1060
Median=86
Type II
Frequency
N_C (at.ppm)
0
1000
2000
3000
4000
20
10
200
100
800
600
400

Figure 3

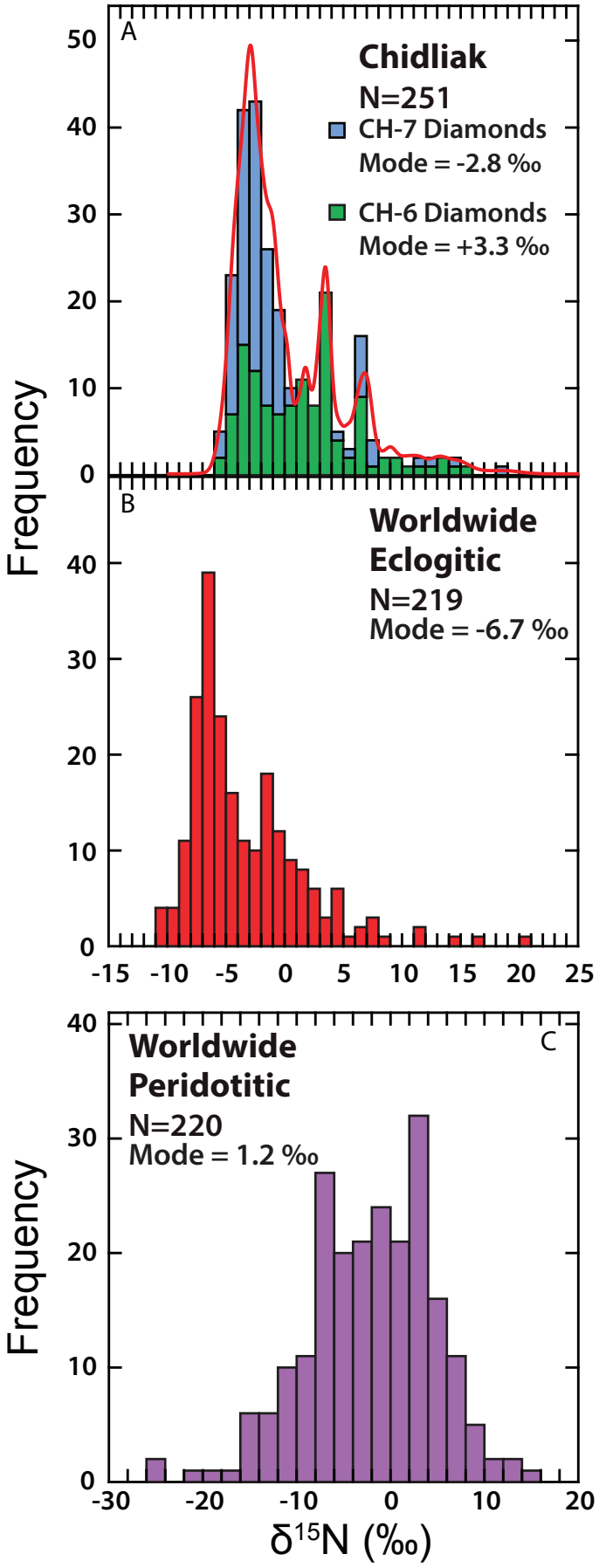
A
Chidliak
N=251
CH-7 Diamonds
Mode = -2.8 ‰
CH-6 Diamonds
Mode = +3.3 ‰
B
Worldwide
Eclogitic
N=219
Mode = -6.7 ‰
C
Worldwide
Peridotitic
N=220
Mode = 1.2 ‰
Frequency
δ15N (‰)

Figure 4

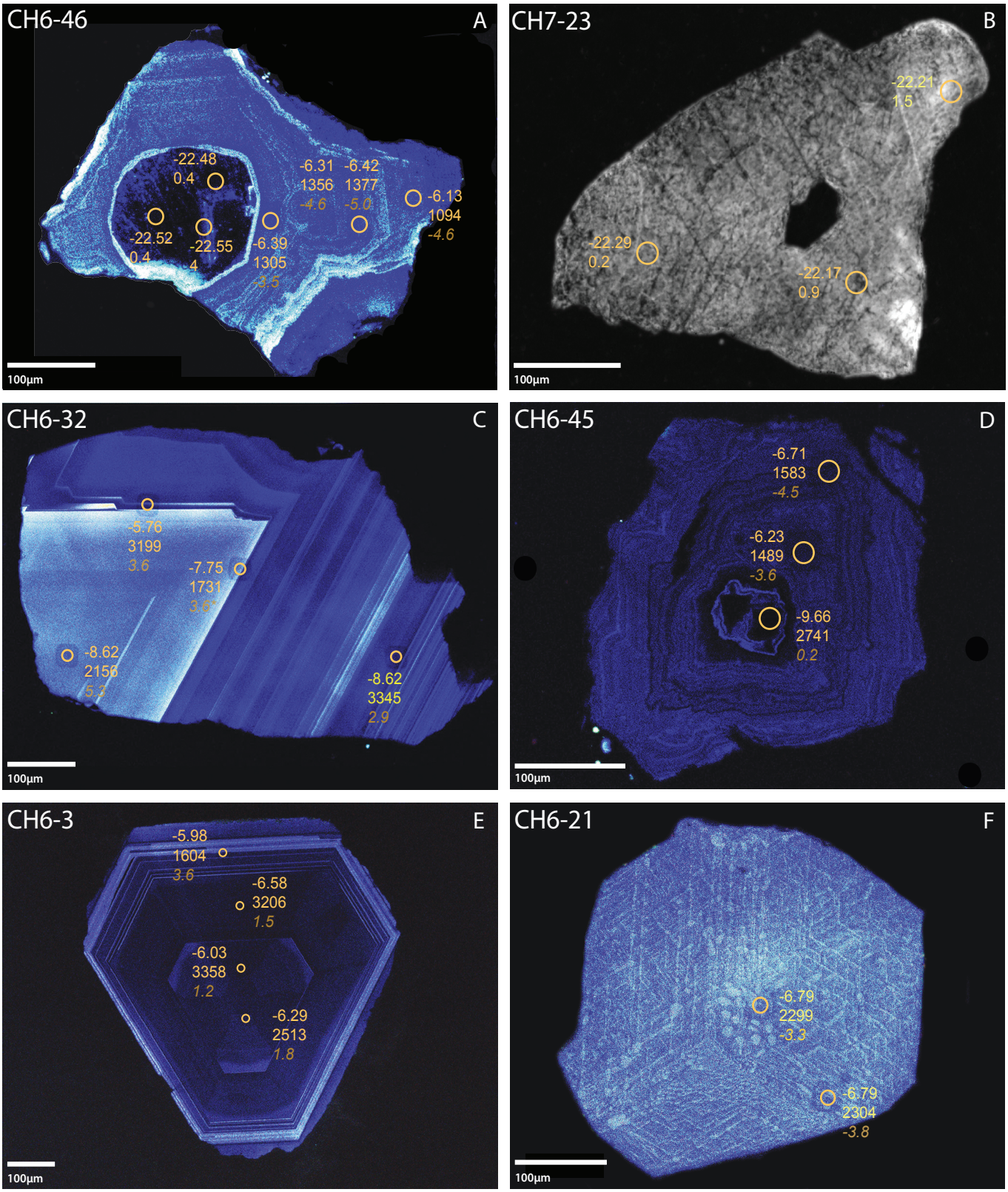
CH6-46
A
-22.48
0.4
-22.52
0.4
-22.55
4
-6.39
1305
-3.5
-6.31
1356
-4.6
-6.42
1377
-5.0
-6.13
1094
-4.6
100µm
CH7-23
B
-22.21
1.5
-22.29
0.2
-22.17
0.9
100µm
CH6-32
C
-5.76
3199
3.6
-7.75
1731
3.6*
-8.62
2156
5.7
-8.62
3345
2.9
100µm
CH6-45
D
-6.71
1583
-4.5
-6.23
1489
-3.6
-9.66
2741
0.2
100µm
CH6-3
E
-5.98
1604
3.6
-6.58
3206
1.5
-6.03
3358
1.2
-6.29
2513
1.8
100µm
CH6-21
F
-6.79
2299
-3.3
-6.79
2304
-3.8
100µm

Figure 5

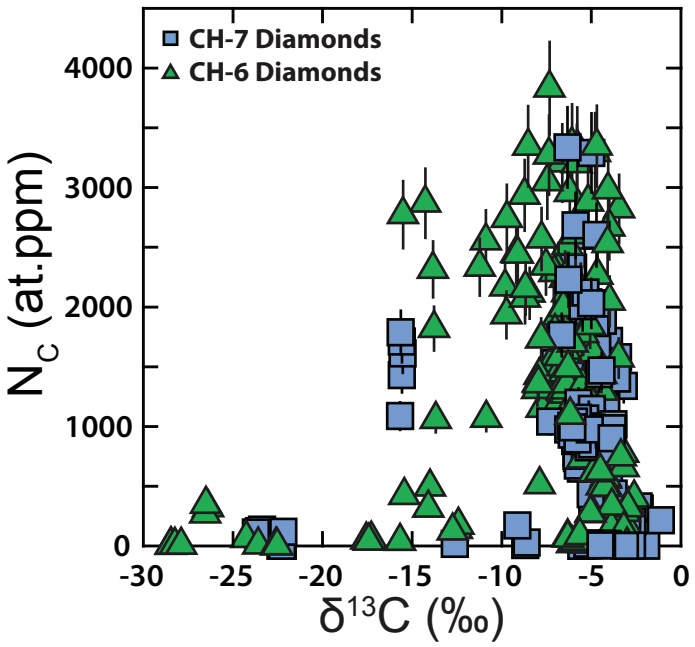
CH-7 Diamonds
CH-6 Diamonds
4000
3000
2000
1000
0
-30
-25
-20
-15
-10
-5
0
N_C (at.ppm)
$\delta^{13}C$ (‰)

Figure 6

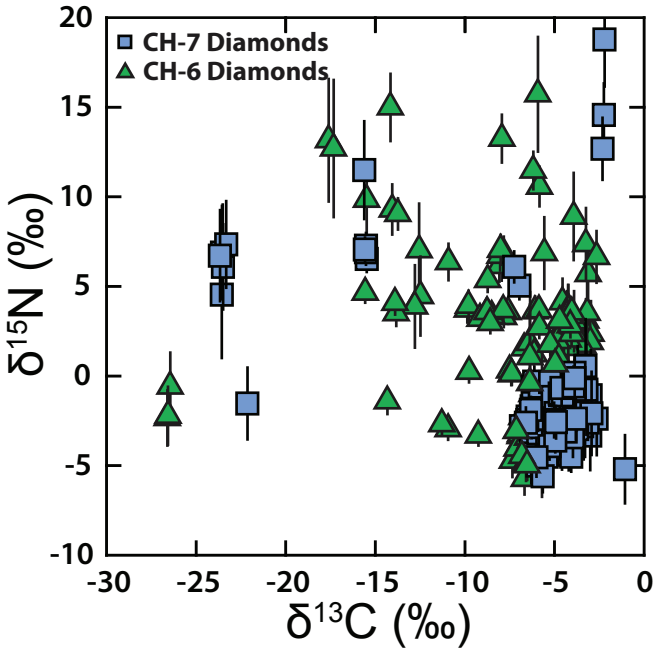
CH-7 Diamonds
CH-6 Diamonds
20
15
10
5
0
-5
-10
-30
-25
-20
-15
-10
-5
0
δ15N (‰)
δ13C (‰)

Figure 7

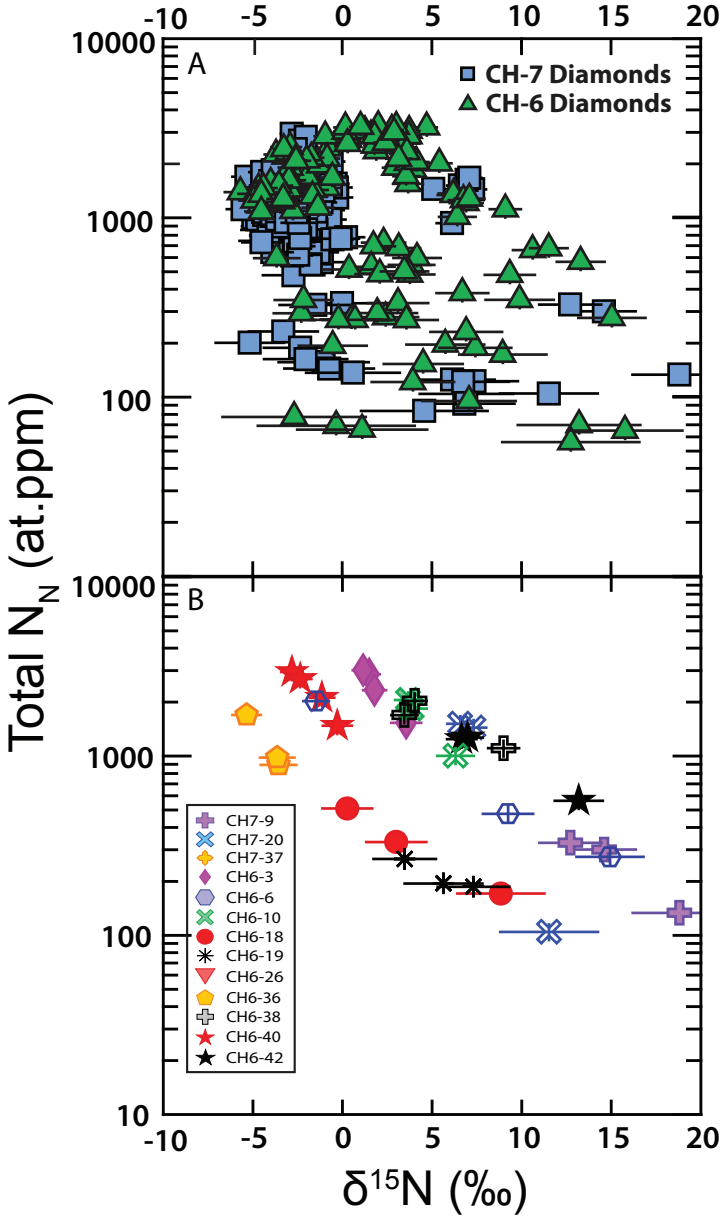
A
CH-7 Diamonds
CH-6 Diamonds
B
CH7-9
CH7-20
CH7-37
CH6-3
CH6-6
CH6-10
CH6-18
CH6-19
CH6-26
CH6-36
CH6-38
CH6-40
CH6-42
Total N_N (at.ppm)
$\delta^{15}N$ (‰)
10000
1000
100
10
-10
-5
0
5
10
15
20

Figure 8

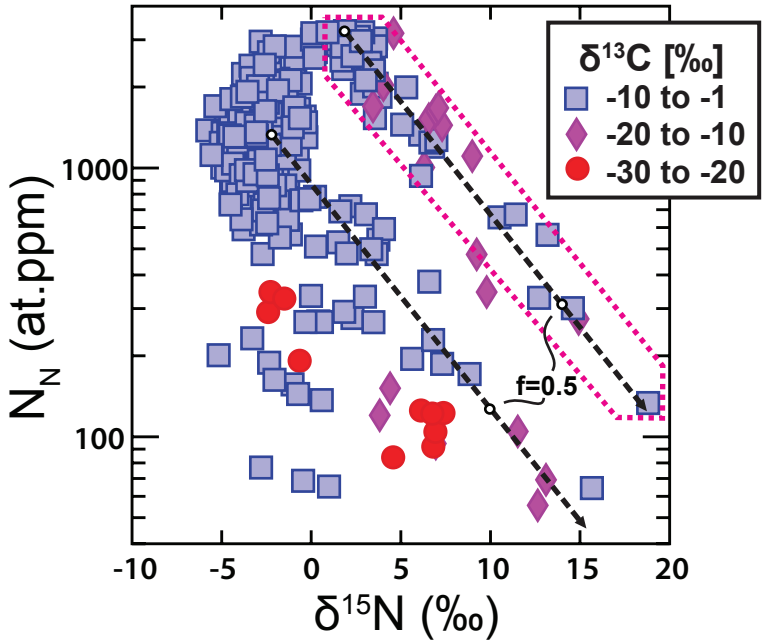
δ13C [‰]
-10 to -1
-20 to -10
-30 to -20
f=0.5
1000
100
-10
-5
0
5
10
15
20
NN (at.ppm)
δ15N (‰)

Figure 9

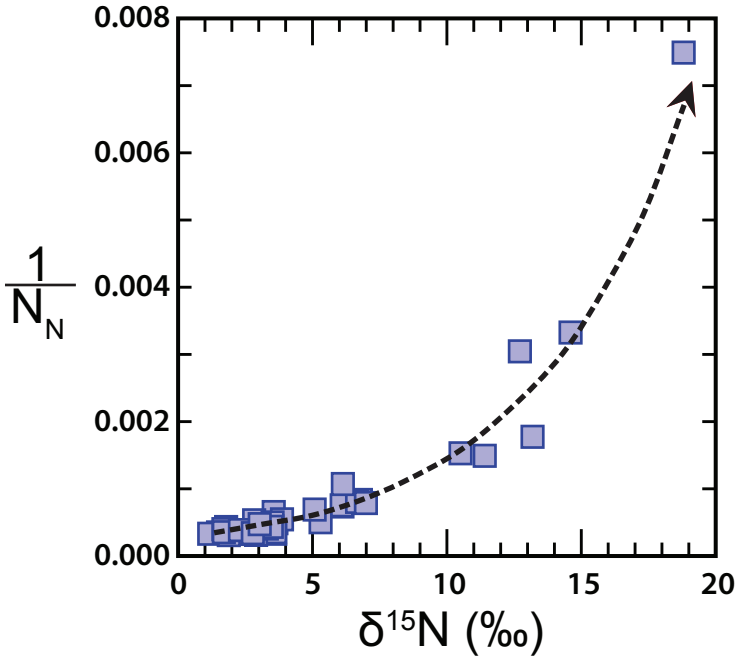

Figure 10

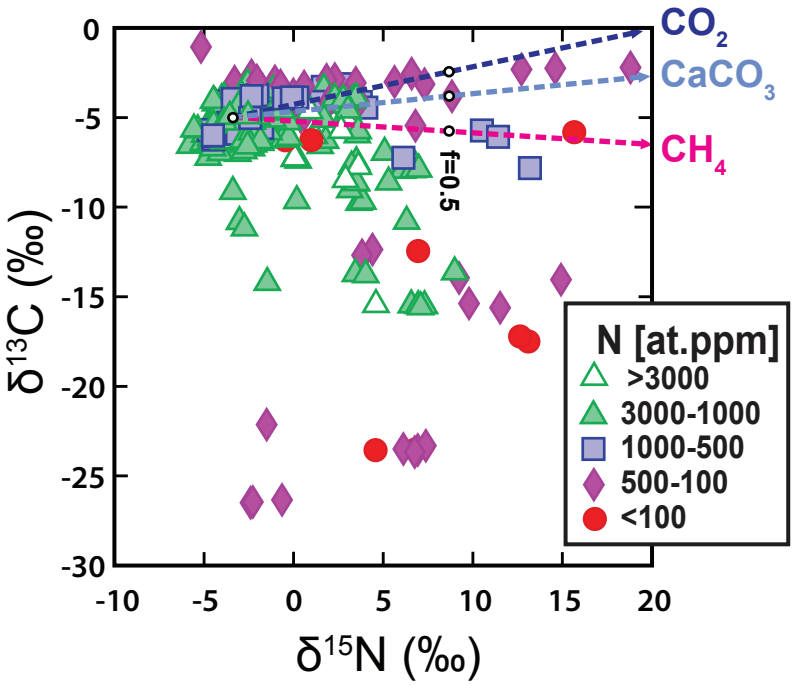
CO2
CaCO3
CH4
f=0.5
N [at.ppm]
>3000
3000-1000
1000-500
500-100
<100
δ13C (‰)
δ15N (‰)
0
-5
-10
-15
-20
-25
-30
-10
-5
0
5
10
15
20

Figure 11

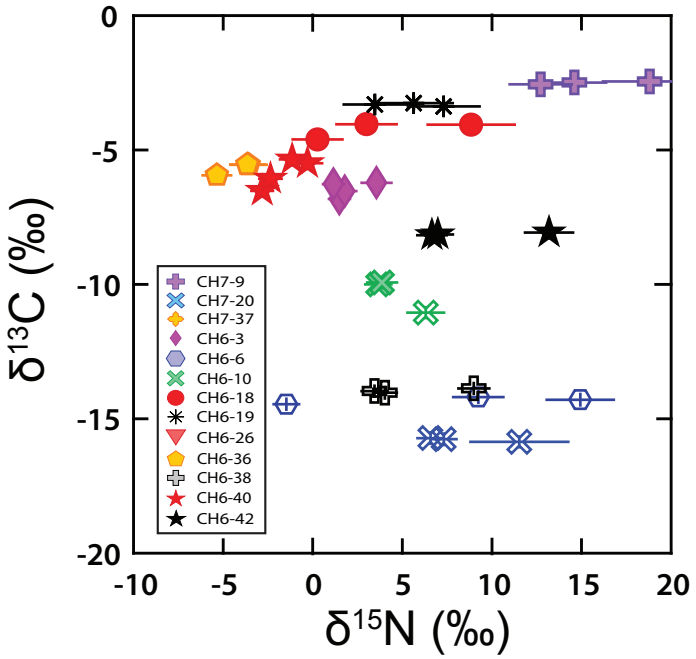
0
-5
-10
-15
-20
-10
-5
0
5
10
15
20
δ13C (‰)
δ15N (‰)
CH7-9
CH7-20
CH7-37
CH6-3
CH6-6
CH6-10
CH6-18
CH6-19
CH6-26
CH6-36
CH6-38
CH6-40
CH6-42

Table 1.1
Click here to download Table: Table 1.1.xlsx

Table 1. Compilation of $\delta^{13}C$, $\delta^{15}N$ and nitrogen contents measured via SIMS for 94 Chidliak diamonds

Sample ID	SIMS ID	$\delta^{13}C$ (‰) (VPDB)	2σ (‰)	N_C (at.ppm)	$\delta^{15}N$ (‰) (AIR)	2σ (‰)	N_N (at.ppm)	CL type
CH6-1	S1989	-3.17	0.20	775	2.19	1.20	721	agate-like banding
CH6-1	S1989	-3.14	0.21	656	3.05	1.18	673	
CH6-1	S1989	-3.29	0.21	745	1.63	1.19	688	
CH6-2	S1990	-6.63	0.21	1760	-3.15	0.74	1738	complex
CH6-2	S1990	-6.80	0.21	1851	-2.87	0.80	1685	
CH6-2	S1990	-6.71	0.21	1767	-2.35	0.79	1799	
CH6-3	S1991	-5.98	0.21	1604	3.56	0.83	1533	complex
CH6-3	S1991	-6.58	0.21	3206	1.49	0.58	2861	
CH6-3	S1991	-6.29	0.20	2513	1.79	0.64	2333	
CH6-3	S1991	-6.03	0.21	3358	1.16	0.58	3019	
CH6-4	S1992	-5.83	0.21	2604	-0.89	0.75	2423	cuboid
CH6-4	S1992	-6.07	0.20	1706	-1.67	0.84	1522	
CH6-4	S1992	-7.24	0.21	1517	-4.77	0.92	1446	
CH6-5	S1993	-3.04	0.21	3.9				complex
CH6-5	S1993	-2.86	0.21	343	2.31	1.82	277	
CH6-5	S1993	-2.90	0.20	319	1.84	2.21	292	
CH6-6	S1994	-14.22	0.20	2869	-1.47	0.71	2028	octahedral
CH6-6	S1994	-13.95	0.21	492	9.24	1.40	477	
CH6-6	S1994	-14.05	0.21	315	14.93	1.87	274	
CH6-7	S1995	-24.20	0.21	61				hiatus
CH6-7	S1995	-23.53	0.20	7.1				
CH6-7	S1995	-4.85	0.20	1616	-0.96	0.79	1454	
CH6-7	S1995	-3.42	0.21	1573	-1.72	0.80	1418	
CH6-8	S1996	-15.46	0.20	2773	4.60	0.56	3169	octahedral
CH6-8	S1996	-15.62	0.21	37				
CH6-8	S1996	-15.38	0.21	422	9.79	1.90	345	
CH6-9	S1997	-7.73	0.21	1151	6.80	0.92	1199	agate-like banding
CH6-9	S1997	-7.84	0.21	1427	6.12	0.85	1357	
CH6-9	S1997	-7.97	0.20	1309	6.09	0.88	1330	
CH6-10	S1998	-9.76	0.20	2167	3.66	0.73	2058	agate-like banding
CH6-10	S1998	-9.69	0.21	1935	3.87	0.83	1839	
CH6-10	S1998	-10.81	0.20	1068	6.31	1.02	1004	
CH6-11	S1999	-6.41	0.21	1706	-2.79	0.68	1654	complex
CH6-11	S1999	-6.39	0.21	1639	-2.05	0.68	1683	
CH6-11	S1999	-6.06	0.20	1051	-3.06	0.70	1426	
CH6-12	S2000	-6.81	0.20	1159	-3.41	0.94	1206	cuboid
CH6-12	S2000	-6.82	0.21	1186	-3.89	1.08	1191	
CH6-12	S2000	-6.60	0.20	1300	-2.86	1.05	1084	
CH6-13	S2001	-3.40	0.20	2821	1.69	0.57	2511	complex
CH6-13*	S2001	-4.32	0.20	1294	2.83	0.67	1888	
CH6-13	S2001	-6.81	0.20	1924	-3.02	0.63	1890	
CH6-14	S2002	-5.37	0.21	16				homogeneous
CH6-14	S2002	-6.02	0.21	18				

Table1.2

Click here to download Table: Table 1.2.xlsx

Sample ID	SIMS ID	$\delta^{13}C$ (‰) (VPDB)	2σ (‰)	N_C (at.ppm)	$\delta^{15}N$ (‰) (AIR)	2σ (‰)	N_N (at.ppm)	CL-Type
CH6-15	S2003	-26.34	0.21	318	-0.64	1.90	192	cuboid
CH6-15	S2003	-26.50	0.21	268	-2.40	1.53	291	
CH6-15	S2003	-26.46	0.21	348	-2.27	1.61	345	
CH6-16	S2004	-28.40	0.21	6.1				homogeneous
CH6-16	S2004	-28.40	0.20	5.6				
CH6-16	S2004	-28.40	0.21	5.8				
CH6-17	S2005	-4.13	0.20	558	1.51	1.29	528	homogeneous
CH6-17	S2005	-4.14	0.21	573	3.75	1.27	541	
CH6-17	S2005	-4.45	0.20	624	4.06	1.32	592	
CH6-18	S2006	-3.82	0.20	150	8.84	2.43	171	octahedral
CH6-18	S2006	-3.80	0.21	333	3.00	1.68	332	
CH6-18	S2006	-4.37	0.21	502	0.27	1.39	510	
CH6-19	S2007	-3.02	0.21	176	5.64	2.17	195	homogeneous
CH6-19	S2007	-3.14	0.20	139	7.31	2.00	187	
CH6-19	S2007	-3.07	0.20	280	3.47	1.74	267	
CH6-20	S2008	-6.57	0.20	1500	-5.79	0.88	1378	cuboid
CH6-20	S2008	-6.48	0.20	1447	-4.94	0.97	1350	
CH6-20	S2008	-6.39	0.21	1270	-4.70	0.95	1161	
CH6-21	S2009	-6.79	0.21	2299	-3.30	0.65	2181	complex
CH6-21	S2009	-6.79	0.21	2304	-3.80	0.63	2238	
CH6-22	S2010	-5.12	0.21	2049	-1.36	0.67	1947	agate-like banding
CH6-22	S2010	-6.15	0.21	2958	-1.05	0.59	2824	
CH6-22	S2010	-5.54	0.20	2147	-0.95	0.65	2122	
CH6-23	S2011	-6.41	0.21	2239	-1.83	0.65	2148	cuboid
CH6-23	S2011	-6.29	0.21	2119	-2.09	0.66	2076	
CH6-23	S2011	-7.02	0.20	2287	-3.11	0.67	2295	
CH6-24	S2012	-4.96	0.20	279	0.40	1.71	268	homogeneous
CH6-24	S2012	-4.86	0.20	270	0.60	1.83	267	
CH6-24	S2012	-4.99	0.21	275	-0.32	1.60	267	
CH6-26	S2014	-7.93	0.20	1366	6.66	0.82	1244	homogeneous
CH6-26	S2014	-7.90	0.21	1357	6.99	0.83	1269	
CH6-26	S2014	-7.83	0.21	512	13.19	1.34	564	
CH6-27	S2015	-8.67	0.21	2935	3.48	0.55	2816	octahedral
CH6-27	S2015	-7.48	0.21	2342	3.51	0.65	2272	
CH6-27	S2015	-7.73	0.20	2570	3.24	0.56	2500	
CH6-28	S2016	-10.83	0.20	2552	-3.02	0.59	2462	cuboid
CH6-28	S2016	-9.14	0.21	2449	-3.38	0.56	2402	
CH6-28	S2016	-11.18	0.20	2333	-2.74	0.60	2078	
CH6-29	S2017	-12.45	0.21	138	6.96	2.61	94	homogeneous
CH6-29	S2017	-12.37	0.21	172	4.40	2.21	151	
CH6-29	S2017	-12.69	0.21	125	3.83	2.30	120	
CH6-30	S2018	-8.40	0.20	2115	3.30	0.58	2179	agate-like banding
CH6-30	S2018	-9.05	0.21	2442	3.14	0.58	2129	
CH6-30	S2018	-8.65	0.34	2074	3.52	0.59	2010	

Table1.3

Click here to download Table: Table 1.3.xlsx

Sample ID	SIMS ID	$\delta^{13}C$ (‰) (VPDB)	2σ (‰)	N_C (at.ppm)	$\delta^{15}N$ (‰) (AIR)	2σ (‰)	N_N (at.ppm)	CL-Type
CH6-32	S2020A	-8.62	0.20	2156	5.30	0.67	1995	octahedral
CH6-32*	S2020A	-7.75	0.20	1731	3.62	0.57	3033	
CH6-32	S2020A	-5.76	0.20	3199	3.61	0.59	2834	
CH6-32	S2020A	-8.48	0.21	3345	2.90	0.56	3195	
CH6-33	S2022	-7.40	0.20	3048	0.26	0.58	2698	homogeneous
CH6-33	S2022	-7.31	0.21	3271	0.04	0.60	3002	
CH6-33	S2022	-7.28	0.20	3833	0.07	0.62	3171	
CH6-34	S2023	-17.50	0.21	49	13.10	3.42	69	homogeneous
CH6-34	S2023	-17.22	0.21	56	12.64	3.82	56	
CH6-34	S2023	-17.36	0.20	40				
CH6-35	S2024	-5.40	0.21	1777	-2.97	0.76	1607	cuboid
CH6-35	S2024	-5.99	0.21	1699	-3.08	0.79	1602	
CH6-35	S2024	-6.98	0.20	1792	-4.10	0.86	1554	
CH6-37	S2025	-4.12	0.21	499	3.66	1.36	478	homogeneous
CH6-37	S2025	-4.13	0.20	487	1.98	1.35	481	
CH6-37	S2025	-4.18	0.22	491	3.36	1.32	498	
CH6-38	S2026	-13.63	0.20	1058	8.99	0.86	1107	homogeneous
CH6-38	S2026	-13.73	0.20	1820	3.45	0.72	1694	
CH6-38	S2026	-13.79	0.21	2315	4.03	0.66	2032	
CH6-39	S2027	-5.82	0.21	40	15.67	3.20	64	complex
CH6-39	S2027	-5.73	0.20	1217	10.51	1.10	655	
CH6-39	S2027	-6.08	0.20	1179	11.41	1.05	671	
CH6-40	S2028	-2.55	0.21	401	6.59	1.44	377	complex
CH6-40	S2028	-2.88	0.21	8.7				
CH6-40	S2028	-2.95	0.20	7.0				
CH6-42	S2030	-6.27	0.20	76	-0.45	4.38	68	complex
CH6-42	S2030	-6.26	0.21	65	1.00	3.63	65	
CH6-42	S2030	-5.59	0.20	86	-2.80	3.99	77	
CH6-43	S2031	-5.74	0.21	3336	2.66	0.59	3070	complex
CH6-43	S2031	-4.74	0.20	3291	1.89	0.58	3228	
CH6-43	S2031	-5.13	0.20	2878	1.70	0.61	2827	
CH6-45	S2033	-9.66	0.21	2741	0.18	0.60	2567	cuboid
CH6-45	S2033	-6.23	0.21	1489	-3.64	0.72	1500	
CH6-45	S2033	-6.71	0.20	1583	-4.51	0.73	1454	
CH6-46	S2034	-22.55	0.21	4.0				hiatus
CH6-46	S2034	-6.42	0.21	1377	-5.04	0.82	1239	
CH6-46	S2034	-22.52	0.21	0.4				
CH6-46	S2034	-22.48	0.20	0.4				
CH6-46	S2034	-6.39	0.21	1305	-3.49	0.82	1228	
CH6-46	S2034	-6.31	0.20	1356	-4.63	0.80	1335	
CH6-46	S2034	-6.13	0.21	1094	-4.63	0.90	1075	
CH6-47	S2035	-28.42	0.20	4.3				complex
CH6-47	S2035	-28.18	0.21	5.5				
CH6-47	S2035	-27.84	0.21	5.6				

Table1.4

Click here to download Table: Table 1.4.xlsx

Sample ID	SIMS ID	$\delta^{13}C$ (‰) (VPDB)	2σ (‰)	N_C (at.ppm)	$\delta^{15}N$ (‰) (AIR)	2σ (‰)	N_N (at.ppm)	CL-Type
CH6-48	S2036	-4.04	0.22	2531	3.30	0.65	2458	agate-like banding
CH6-48	S2036	-3.93	0.20	2048	3.49	0.67	2308	
CH6-48	S2036	-3.94	0.21	2668	2.30	0.62	2605	
CH6-48	S2036	-4.01	0.20	2980	2.78	0.68	2964	
CH6-49	S2037	-6.50	0.21	1994	-2.69	0.76	2061	octahedral
CH6-49	S2037	-4.64	0.21	3347	0.91	0.57	3196	
CH6-49	S2037	-4.60	0.22	2265	3.04	0.69	2117	
CH6-50	S2038	-5.44	0.21	1348	-1.78	0.80	1304	cuboid
CH6-50	S2038	-5.06	0.21	1228	-1.47	0.85	1131	
CH6-50	S2038	-5.02	0.20	1844	-0.67	0.70	1661	
CH6-51	S2039	-4.81	0.21	611	-3.77	1.25	591	complex
CH6-51	S2039	-4.39	0.20	1434	-3.40	0.87	1264	
CH6-51	S2039	-5.46	0.20	728	6.80	2.00	229	
CH7-1	S2040	-5.66	0.20	1245	-3.39	1.08	1169	complex
CH7-1	S2040	-5.71	0.20	1219	-3.37	0.94	1146	
CH7-1	S2040	-6.18	0.21	1455	-3.41	0.94	1309	
CH7-2	S2041	-5.66	0.21	931	-3.80	1.09	866	agate-like banding
CH7-2	S2041	-5.02	0.21	906	-3.29	1.08	887	
CH7-2	S2041	-5.07	0.21	830	-2.10	1.22	820	
CH7-3	S2042	-2.98	0.21	188	-1.04	2.51	157	homogeneous
CH7-3	S2042	-3.01	0.20	240	-3.29	1.92	232	
CH7-4	S2043B	-5.30	0.20	741	-2.76	1.19	725	complex
CH7-4	S2043B	-4.96	0.21	16				
CH7-4	S2043B	-5.53	0.21	1184	-1.80	0.96	1117	
CH7-5	S2045	-4.04	0.20	5.0				complex
CH7-5	S2045	-5.51	0.21	1.4				
CH7-5	S2045	-5.15	0.20	4.2				
CH7-6	S2046	-6.87	0.21	1397	-2.77	0.71	1342	complex
CH7-6	S2046	-5.84	0.21	879	-2.02	1.01	714	
CH7-6	S2046	-5.29	0.22	1066	-1.49	0.84	1027	
CH7-7	S2047	-5.96	0.21	2329	-3.35	0.57	2160	complex
CH7-7	S2047	-5.82	0.21	2114	-2.97	0.60	2014	
CH7-7	S2047	-5.31	0.20	2597	-2.28	0.56	2541	
CH7-8	S2048	-5.09	0.21	1090	-0.75	0.83	1105	homogeneous
CH7-8	S2048	-5.04	0.21	974	-1.28	0.85	926	
CH7-8	S2048	-5.16	0.21	1001	-0.66	0.84	978	
CH7-9	S2049	-2.21	0.21	160	18.81	2.61	133	homogeneous
CH7-9	S2049	-2.25	0.22	312	14.60	1.77	301	
CH7-9	S2049	-2.32	0.21	330	12.72	1.73	329	
CH7-10	S2050	-1.92	0.20	3.3				homogeneous
CH7-10	S2050	-1.88	0.21	2.4				
CH7-11	S2051	-4.59	0.21	1159	-4.30	0.88	1123	homogeneous
CH7-11	S2051	-4.62	0.21	1340	-3.97	0.83	1300	
CH7-12	S2052	-2.65	0.20	204	-2.34	2.03	189	complex

Table1.5

Click here to download Table: Table 1.5.xlsx

Sample ID	SIMS ID	$\delta^{13}C$ (‰) (VPDB)	2σ (‰)	N_C (at.ppm)	$\delta^{15}N$ (‰) (AIR)	2σ (‰)	N_N (at.ppm)	CL-Type
CH7-12	S2052	-3.16	0.20	12				
CH7-13	S2053	-3.96	0.20	638	-1.13	1.20	566	octahedral
CH7-13	S2053	-3.71	0.21	1018	-1.44	0.99	860	
CH7-13	S2053	-4.94	0.20	991	-3.05	0.90	971	
CH7-15	S2055	-12.57	0.20	17				complex
CH7-15	S2055	-6.96	0.20	1529	5.08	0.76	1450	
CH7-15	S2055	-7.25	0.21	1041	6.13	0.86	935	
CH7-16	S2056	-6.23	0.21	975	-4.47	1.13	898	complex
CH7-16	S2056	-6.04	0.21	931	-4.39	1.23	858	
CH7-16	S2056	-6.06	0.21	1006	-4.48	1.26	744	
CH7-17	S2057	-6.05	0.20	1254	-3.93	0.89	1109	homogeneous
CH7-17	S2057	-6.02	0.20	1191	-3.68	0.92	1078	
CH7-17	S2057	-6.33	0.20	1157	-3.86	0.92	1073	
CH7-18	S2058	-4.03	0.22	1688	-0.36	0.70	1552	cuboid
CH7-18	S2058	-6.50	0.20	1164	-2.23	0.86	1056	
CH7-18	S2058	-6.27	0.20	1245	-1.66	0.79	1158	
CH7-19	S2059	-5.05	0.21	795	-1.83	0.98	750	complex
CH7-19	S2059	-5.09	0.21	826	-2.39	0.95	789	
CH7-19	S2059	-4.71	0.21	708	-1.30	1.05	641	
CH7-20	S2060	-15.62	0.20	1087	11.53	2.73	105	homogeneous
CH7-20	S2060	-15.52	0.21	1430	7.31	0.71	1442	
CH7-20	S2060	-15.48	0.21	1612	6.57	0.72	1516	
CH7-21	S2061	-5.61	0.21	890	-2.87	1.00	934	complex
CH7-21	S2061	-4.92	0.20	849	-2.18	0.85	995	
CH7-21	S2061	-5.12	0.21	1115	-1.47	0.80	1084	
CH7-22	S2062	-15.52	0.20	1711	6.95	0.70	1630	homogeneous
CH7-22	S2062	-15.58	0.20	1788	7.09	0.68	1673	
CH7-23	S2063	-22.29	0.20	0.2				homogeneous
CH7-23	S2063	-22.17	0.21	0.9				
CH7-23	S2063	-22.21	0.20	1.5				
CH7-24	S2064	-3.46	0.20	1579	-2.76	0.75	1385	complex
CH7-24	S2064	-3.89	0.20	1547	-3.88	0.82	1430	
CH7-24	S2064	-3.14	0.21	1340	-2.56	0.83	1114	
CH7-25	S2065	-5.80	0.22	1336	-3.98	0.88	1372	complex
CH7-25	S2065	-5.95	0.21	1088	-4.96	0.96	1002	
CH7-25	S2065	-5.70	0.21	1073	-4.75	0.90	980	
CH7-26	S2066	-4.44	0.21	1179	-4.07	0.84	1085	octahedral
CH7-26	S2066	-4.21	0.21	1247	-4.36	0.85	1038	
CH7-26	S2066	-4.33	0.20	1247	-3.05	0.91	1039	
CH7-27	S2067	-3.97	0.21	1716	-4.01	0.78	1418	complex
CH7-27	S2067	-4.11	0.21	1177	-3.93	1.08	940	
CH7-27	S2067	-3.71	0.20	438	-0.01	1.72	334	
CH7-28	S2068	-4.31	0.20	1884	-4.01	0.75	1529	complex
CH7-28	S2068	-4.07	0.21	1494	-4.47	0.83	1344	

Table1.6

Click here to download Table: Table 1.6.xlsx

Sample ID	SIMS ID	$\delta^{13}C$ (‰) (VPDB)	2σ (‰)	N_C (at.ppm)	$\delta^{15}N$ (‰) (AIR)	2σ (‰)	N_N (at.ppm)	CL-Type
CH7-28	S2068	-3.73	0.22	973	-2.92	0.89	1063	
CH7-30	S2069	-6.22	0.20	2228	-0.59	0.69	2061	complex
CH7-30	S2069	-6.13	0.20	1448	-0.27	0.81	1299	
CH7-30	S2069	-5.82	0.21	2042	-1.36	0.75	1913	
CH7-31	S2070	-3.51	0.20	1401	-1.15	0.79	1220	complex
CH7-31	S2070	-3.97	0.21	931	-3.39	1.08	860	
CH7-31	S2070	-3.76	0.20	985	-2.01	0.97	861	
CH7-32	S2071	-5.16	0.21	19				complex
CH7-32	S2071	-4.89	0.21	337	-2.71	1.71	478	
CH7-32	S2071	-4.98	0.22	434				
CH7-33	S2072	-23.52	0.20	97	6.82	2.79	92	hiatus
CH7-33	S2072	-5.59	0.21	682	-1.75	1.15	551	
CH7-33	S2072	-5.76	0.21	784	-2.59	1.04	732	
CH7-33	S2072	-5.52	0.21	647	-2.79	1.10	616	
CH7-33	S2072	-23.57	0.21	98	4.58	3.54	84	
CH7-33	S2072	-5.75	0.20	735	-2.68	1.11	695	
CH7-33	S2072	-23.56	0.21	97	6.93	2.60	104	
CH7-34	S2073	-23.50	0.21	122	6.13	2.37	125	homogeneous
CH7-34	S2073	-23.32	0.21	135	7.38	2.42	123	
CH7-34	S2073	-23.67	0.20	111	6.76	2.54	122	
CH7-35	S2074	-5.70	0.20	673	-2.45	1.19	622	hiatus
CH7-35	S2074	-5.77	0.21	754	-3.89	1.13	644	
CH7-35*	S2074	-22.14	0.22	119	-1.50	2.01	327	
CH7-35	S2074	-5.72	0.20	891	-4.11	1.03	797	
CH7-36	S2075	-5.70	0.21	1963	-5.35	0.79	1697	complex
CH7-36	S2075	-5.31	0.21	793	-3.57	0.99	894	
CH7-36	S2075	-5.30	0.20	1143	-3.64	0.96	981	
CH7-37	S2076	-3.22	0.21	159	-0.73	2.49	144	homogeneous
CH7-37	S2076	-3.27	0.21	147	0.59	2.61	137	
CH7-37	S2076	-2.94	0.21	171	-2.04	2.32	163	
CH7-38	S2077	-5.22	0.21	1215	-2.29	0.89	1217	homogeneous
CH7-38	S2077	-5.76	0.20	1545	-3.61	0.89	1473	
CH7-38	S2077	-5.86	0.20	1488	-3.10	0.81	1442	
CH7-39	S2078	-6.12	0.20	1451	-4.54	0.85	1320	complex
CH7-39	S2078	-6.09	0.21	1365	-4.28	0.85	1308	
CH7-39	S2078	-5.91	0.20	1041	-3.16	0.97	947	
CH7-40	S2079	-5.25	0.21	1725	-0.29	0.81	1477	octahedral
CH7-40	S2079	-5.11	0.20	2039	-1.14	0.68	2116	
CH7-40	S2079	-6.28	0.20	3336	-2.82	0.60	2947	
CH7-40	S2079	-5.83	0.20	2684	-2.36	0.62	2695	
CH7-42	S2081	-6.52	0.21	1836	-2.42	0.74	1749	complex
CH7-42	S2081	-6.32	0.20	2053	-1.85	0.72	1943	
CH7-42	S2081	-6.60	0.21	1766	-2.57	0.85	1626	
CH7-43	S2082	-4.95	0.20	3290	-2.03	0.60	2832	cuboid

Table1.7

Click here to download Table: Table 1.7.xlsx

Sample ID	SIMS ID	$\delta^{13}C$ (‰) (VPDB)	2σ (‰)	N_C (at.ppm)	$\delta^{15}N$ (‰) (AIR)	2σ (‰)	N_N (at.ppm)	CL-Type
CH7-43	S2082	-4.69	0.20	1907	-1.03	0.78	1561	
CH7-43	S2082	-4.71	0.21	1814	-0.94	0.80	1679	
CH7-44	S2083	-4.66	0.20	2602	-2.59	0.64	2420	homogeneous
CH7-44	S2083	-4.54	0.20	1548	-1.03	0.81	1416	
CH7-44	S2083	-4.61	0.20	1649	-0.63	0.93	1531	
CH7-45	S2084	-8.63	0.20	7.7				complex
CH7-45	S2084	-8.56	0.20	28				
CH7-45	S2084	-9.07	0.20	171				
CH7-46	S2085	-3.88	0.21	806	0.22	1.00	780	homogeneous
CH7-46	S2085	-3.94	0.20	803	-0.54	1.11	758	
CH7-46	S2085	-3.88	0.21	806	-0.09	1.01	765	
CH7-47	S2086	-4.52	0.21	1437	-3.03	0.95	1315	octahedral
CH7-47	S2086	-4.38	0.20	1468	-3.06	0.87	1354	
CH7-47	S2086	-3.81	0.20	901	-2.34	1.15	772	
CH7-48	S2087	-5.44	0.21	2007	-4.46	0.73	1802	complex
CH7-48	S2087	-5.28	0.20	2121	-3.87	0.75	1843	
CH7-48	S2087	-4.96	0.21	2030	-3.56	0.65	1921	
CH7-49	S2088	-1.07	0.21	214	-5.16	1.90	201	complex
CH7-49	S2088	-2.68	0.20	1.7				
CH7-49	S2088	-4.03	0.21	17				
CH7-50	S2089	-3.07	0.21	0.7				complex
CH7-50	S2089	-4.35	0.21	20				
CH7-50	S2089	-4.43	0.20	4.5				
CH7-51	S2090	-5.03	0.21	975	-2.42	0.96	938	complex
CH7-51	S2090	-4.92	0.21	1147	-2.54	0.90	1074	
CH7-51	S2090	-5.66	0.20	1198	-5.56	0.88	1118	
CH7-51	S2090	-6.01	0.21	992	-4.50	1.08	731	

N_C is the nitrogen content measured on the same spot locations as the $\delta^{13}C$ values, whereas N_N is the nitrogen content measured during $\delta^{15}N$ analysis.

See text for description of the various types of cathodoluminescence observed.

The sample numbers with an * denote measurements where the $\delta^{13}C$ and $\delta^{15}N$ values cannot be compared because the spots cross over important internal boundaries.